

Radiative Transitions in Charmonium from Lattice QCD

Jozef J. Dudek, Robert G. Edwards, and David G. Richards

*Jefferson Laboratory MS 12H2, 12000 Jefferson Avenue, Newport News, VA 23606, USA**

Radiative transitions between charmonium states offer an insight into the internal structure of heavy-quark bound states within QCD. We compute, for the first time within lattice QCD, the transition form-factors of various multiplicities between the lightest few charmonium states. In addition, we compute the experimentally unobservable, but physically interesting vector form-factors of the η_c , J/ψ and χ_{c0} .

To this end we apply an ambitious combination of lattice techniques, computing three-point functions with heavy domain wall fermions on an anisotropic lattice within the quenched approximation. With an anisotropy $\xi = 3$ at $a_s \sim 0.1$ fm we find a reasonable gross spectrum and a hyperfine splitting ~ 90 MeV, which compares favourably with other improved actions.

In general, after extrapolation of lattice data at non-zero Q^2 to the photopoint, our results agree within errors with all well measured experimental values. Furthermore, results are compared with the expectations of simple quark models where we find that many features are in agreement; beyond this we propose the possibility of constraining such models using our extracted values of physically unobservable quantities such as the J/ψ quadrupole moment.

We conclude that our methods are successful and propose to apply them to the problem of radiative transitions involving hybrid mesons, with the eventual goal of predicting hybrid meson photoproduction rates at the GlueX experiment.

PACS numbers: 12.38.Gc, 12.39.Pn, 12.39.Jh, 12.40.Yx, 13.20.Gd, 13.40.Gp, 14.40.Gx

I. INTRODUCTION

Charmonium occupies a valuable intermediate position within QCD, being neither in the purely non-relativistic regime nor the regime where chiral symmetry breaking dominates the physics. This makes it a relatively clean system in which to study non-perturbative QCD dynamics, and indeed QCD-inspired quark-potential models as well as lattice QCD have been rather successful in describing the observed features of the spectrum[1]. However, charmonium cannot be considered to be completely understood; as an example, in recent years a number of new charmonium resonances have been claimed in experiment (see [2] for a review), several of which cannot be easily reconciled with the predictions of simple quark-potential models.

Unlike the light quark sector, in charmonium the lightest state for most J^{PC} 's lies below the threshold for OZI-allowed decay and consequently these states are rather narrow. These states have been the subject of many calculations in lattice QCD which generally reproduce the gross structure of the spectrum, but are unable to account for all of the detailed fine structure (such as the 117 MeV $J/\psi - \eta_c$ splitting), owing to some combination of the approximations inherent in the computations, which can include the finite lattice spacing, quenching and lack of disconnected diagrams.

Masses are not the only well measured charmonium observables. Because of the small total width of these lightest few states, radiative transitions between them

constitute large branching fractions and have been measured experimentally by a number of groups [3, 4]. These quantities have been studied within quark-potential models (and latterly EFT approaches like pNRQCD) where they are related to the overlap of meson wavefunctions with the photon current operator and as such are an insight into the internal structure of these states. QCD sum rules have also been applied with some success[5]. No study of radiative transitions in charmonium has yet been performed using lattice QCD - it is this situation that we remedy in this paper.

This study in the charmonium sector is an ideal test-bed for our eventual aim of computing photocouplings in the light-quark sector, in particular the coupling between a conventional meson, a photon and a hybrid meson. Such a coupling drives the photoproduction mechanism proposed by the GlueX collaboration for their experiment in Hall D of the upgraded CEBAF at Jefferson Lab[6]. Flux-tube model calculations [7, 8] suggest that these couplings are not small and that we may expect copious production of hybrid mesons, but the assumptions underlying such a model need to be tested in a framework closer to QCD. This paper will focus on transitions between conventional charmonium mesons, and we will proceed to transitions to hybrid mesons in a subsequent work.

In section II we outline the computational details of our lattice calculation and in section III we present the charmonium spectrum so obtained. In section IV we explain how three-point functions extracted from the computation can be converted into multipole form-factors and in section V we present lattice estimates for the vector form-factors of the lightest three charmonium states and compare with what one would expect on the basis of simple

*Electronic address: dudek@jlab.org

quark models. In section VI we consider radiative transitions and discuss the extrapolation from the non-zero Q^2 accessible on our finite-volume lattice to the relevant case of an on-shell photon. Finally in section VII we conclude, relegating the details of Lorentz covariant multipole decompositions and scale setting on anisotropic lattices to appendices.

II. COMPUTATIONAL DETAILS

The computations were performed in the quenched approximation to QCD, using the Chroma software system [9]. We employed 300 configurations on a $12^3 \times 48$ lattice generated using an anisotropic Wilson gauge action [10], with a renormalized anisotropy $\xi \equiv a_s/a_t = 3$. The temporal lattice spacing obtained from the static quark-antiquark potential is $a_t^{-1} = 6.05(1)$ GeV.

Anisotropic lattices as applied to charmonium exploit the fact that while the quark mass scale demands a cut-off above ~ 1.5 GeV, the internal three-momentum scale is typically much lower, ~ 500 MeV. On our lattice, we can have both $m_c a_t$ and $|\vec{p}|a_s$ reasonably small and a spatial length $\gtrsim 1$ fm without requiring very many spatial lattice sites. We work on only one volume, $L_s \approx 1.2$ fm; previous charmonium spectrum studies indicate that there are no significant finite volume effects for lattices of this size or larger [11, 12]. With this volume and anisotropy the three-momenta accessible are $\vec{p} = \frac{2\pi}{\xi L_s a_t} (n_x, n_y, n_z) \approx 1.06 \text{ GeV} (n_x, n_y, n_z)$.

The quark propagators were computed using an anisotropic version of the domain-wall fermion (DWF) action [13] with a domain-wall height $a_t M = 1.7$, a fifth dimensional extent $L_5 = 16$, and a quark mass $a_t m_q$. The conventions used for the action are defined in Ref. [14]. In terms of dimensionless variables $\check{\psi} = a_s^{3/2} \psi$ and $\check{W}_\mu = a_\mu W_\mu$, where $a_0 = a_t$ and $a_k = a_s, k = 1, 2, 3$. The kernel of the domain action is the anisotropic Wilson fermion action [15, 16]:

$$a_t Q = -a_t M + \nu_t \check{W}_t \gamma_4 + \frac{\nu_s}{\xi_0} \sum_k \check{W}_k \gamma_k, \quad (1)$$

where the Wilson operator

$$W_\mu \equiv \nabla_\mu - \frac{a_\mu}{2} \gamma_\mu \Delta_\mu.$$

The parameter ξ_0 in Eq. 1 is the bare anisotropy which is determined in the gluonic sector so as to yield the desired renormalized anisotropy ξ . The remaining parameters of the action, m_q, ν_s and ν_t represent the quark mass, and the renormalization of the couplings in the spatial and temporal directions, respectively. The parameters ν_s and ν_t are not independent; we will fix $\nu_t = 1$ and then tune (m_q, ν_s) so as to yield the desired quark mass and such that the speed of light obtained from the meson dispersion relations be 1.0, as discussed in the next section.

While this computation is performed at only a single value of the lattice spacing and hence no attempt can be

made to determine the lattice spacing dependence of the results, an important benefit to the use of the domain-wall fermion action is that it is automatically improved to $\mathcal{O}(a^2)$.

We anticipate that the quenched approximation will not be a serious impediment to this study. In the sub- $D\bar{D}$ -threshold charmonium system we expect (on the basis of previous lattice studies) that the dominant effect of light quarks will be to modify the running of the strong coupling. In the quenched approximation the QCD β function is not properly reproduced, thus if we set our lattice scale using a long distance dominated quantity (such as the $1P - 1S$ splitting or some intermediate distance in the static quark-antiquark potential) then we will have a weakened coupling at short distances compared to QCD. Hence within the quenched approximation we cannot expect to correctly describe such short-distance-dominated quantities as the hyperfine splitting, or meson decay constants [17, 18]. Our principal interest is with radiative transitions, which are dominated by long-distance wavefunction overlaps, and hence should not be considerably distorted by the quenched approximation.

III. SPECTRUM

Charmonium masses and interpolating field overlap factors were extracted from fits to the *connected* two-point functions¹, $\Gamma_{ij}^{(2)}(\vec{p}; t) =$

$$\sum_{\vec{x}} e^{-i\vec{p}\cdot\vec{x}} \langle \bar{\psi} \Gamma_i \psi(\vec{x}, t) \bar{\psi} \Gamma_j \psi(\vec{0}, 0) \rangle = \sum_N \frac{Z_i^{(N)} Z_j^{(N)*}}{2E^{(N)}} e^{-E^{(N)} t} \quad (2)$$

The fact we used local fermion bilinears as interpolating fields limits us to the J^{PC} listed in Table I.

In the previous section we discussed the need to have a rather fine lattice spacing to ensure that charm quarks are not “cut-off”; a related problem arises from the two-scaledness of the charmonium system. The scale which dictates our choice of lattice spacing is the typical mass of a charmonium state ~ 3 GeV, while the level spacing e.g. $J/\psi - \psi' \sim 600$ MeV, is much smaller. This second scale indicates how fast, relatively, the excited state exponentials in eqn (2) fall off with t , which we see will be rather slow, so that it is possible at finite times to get contributions from many excited states. This is not the case with light quarks where the level splitting is of the same size as the ground state mass (e.g. $\rho(770), \rho(1450)$). Because many excited states can be contributing during the finite temporal-extent of our lattice, we are unlikely to reach a plateau and as such extracting the ground-state mass is non-trivial.

¹ Disconnected diagrams will be discussed in section IV

We can reduce this problem somewhat if we improve the overlap of the interpolating field on to the ground state by smearing it over space. We do so using a gauge invariant cubic approximation to a rotationally symmetric Gaussian,

$$\left(1 - \frac{3\sigma^2}{2N}\right)^N \left(1 + \frac{\sigma^2/4N}{1-3\sigma^2/2N} \sum_{i=1}^3 \left[U_{x,i} \delta_{x,x+i} + U_{x-\hat{i},i}^\dagger \delta_{x,x-\hat{i}} \right] \right)^N \xrightarrow{N \rightarrow \infty} e^{-\sigma^2 \nabla^2/4}. \quad (3)$$

With the right smearing radius this will resemble the ground state wavefunction and maximise the overlap, while the excited states, which have radial nodes, will have a decreased overlap.

We computed two-point functions with smearing radii $\sigma = 0.0, 3.6, 4.0$. For the case $\sigma = 3.6$, we attempted to reduce gauge fluctuations by smearing the gauge links entering into eqn. 3 using the gauge-invariant procedure (APE) introduced in ref. [19]. For $\sigma = 3.6, 4.0$ we used $N = 32, 50$ and $5, 0$ APE smearing iterations.

We display effective mass plots in figure 1, where the oscillations in the first few timeslices are an artifact of the non-locality of the DWF action in four dimensions. The $\sigma = 3.6$ smeared-smeared data has reasonable plateaux, at least for the η_c, ψ and χ_{c0} .

Our fitting procedure is as follows. Given a set of interpolating operators $\{O_i\}$, we can construct the matrix of time-sliced correlators

$$\begin{aligned} \Gamma_{ij}^{(2)}(\vec{p}; t) &\equiv \sum_{\vec{x}} e^{-i\vec{p}\cdot\vec{x}} \langle O_i(\vec{x}, t) O_j^\dagger(0) \rangle \\ &= \sum_N \frac{Z_i^{(N)}(\vec{p}) Z_j^{(N)*}(\vec{p})}{2E^{(N)}} e^{-E^{(N)}t}, \end{aligned} \quad (4)$$

where

$$Z_i^{(N)}(\vec{p}) = \langle 0 | O_i | N(\vec{p}) \rangle.$$

If we had computed every element of the $\Gamma_{ij}^{(2)}$, then we could apply a variational method to diagonalise the system. However, in general we have an incomplete matrix, with several sink operators for each source operator. Thus we employ a ‘‘factorizing’’ fit to this incomplete matrix of correlators, in which the fitted parameters are $\{E^{(i)}, Z_j^{(i)} : j = 1, \dots, N_{\text{op}}, i = 1, \dots, N_{\text{exp}}\}$, where there are N_{op} operators used in the fit, and we include N_{exp} states. We assume that the residues of the fit factorize according to eqn. 4 and that as demonstrated in Appendix B, the Z ’s are real. In practice we include the three smearing combinations shown in figure 1 for each J^{PC} and where possible fit to the ground state plus one excited state. For the χ_{c1} and h_c the noise on the data allowed for only inclusion of the ground state in the fit.

In order to propagate statistical error due to the finite number of gauge field configurations through our calculations we adopt a single elimination jackknife procedure.

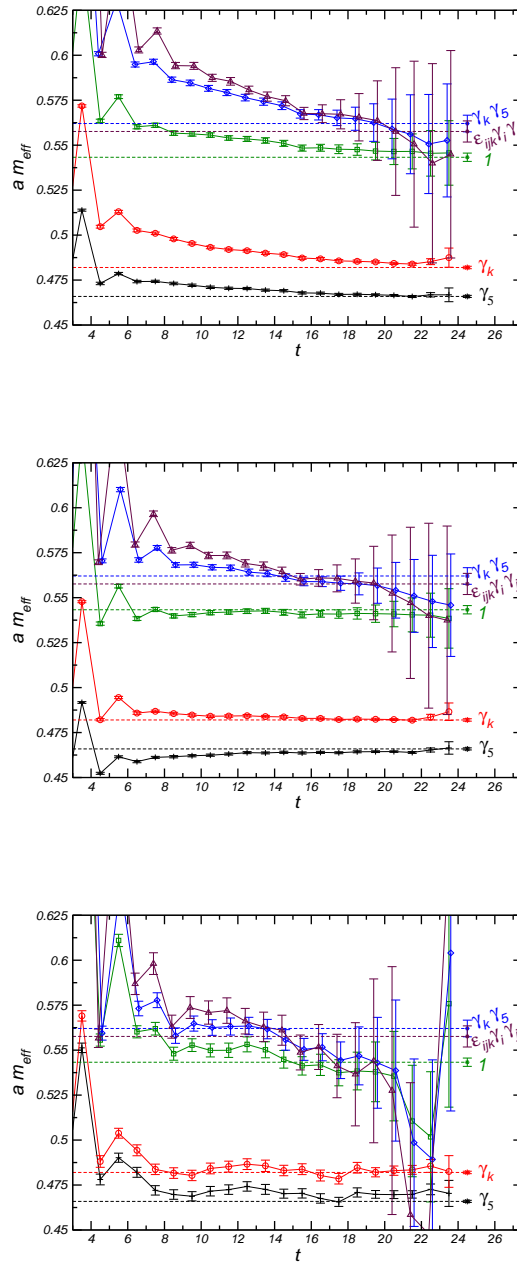


FIG. 1: Effective mass plots (at $\vec{p} = (000)$) using local interpolating fields. Dashed lines and rightmost data point show the ground-state mass obtained from the multi-correlator fit. (a) smeared($\sigma = 4.0$)-local (b) smeared($\sigma = 3.6$)-local (c) smeared($\sigma = 3.6$)-smeared($\sigma = 3.6$)

For the two-point function fits we remove from the ensemble one configuration and average the remaining two-point functions. The factorizing fit is performed on this average yielding a value for each of the fit parameters (Z, E). This is repeated for each configuration yielding an ensemble for the fit parameters over configurations.

These are saved for later use in the three-point function calculations.

Fits are shown in Figure 2 and Table I.

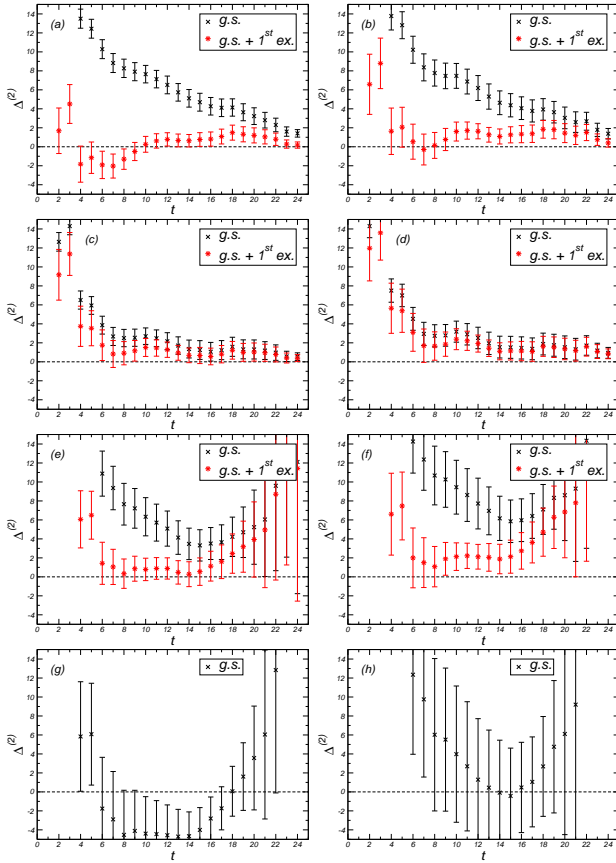


FIG. 2: Data($\sigma = 3.6 - \sigma = 3.6$)-fit percentage deviation, $\Delta^{(2)} \equiv 100 \frac{\text{data} - \text{fit}}{\text{data}}$. Black points indicate the contribution of the ground-state to the fit, the red points include both the ground and first excited states. (a) $\eta_c(\gamma_5)$, $\vec{p} = (000)$, (b) $\eta_c(\gamma_5)$, $\vec{p} = (100)$, (c) $\psi(\gamma_k)$, $\vec{p} = (000)$, (d) $\psi(\gamma_k)$, $\vec{p} = (100)$, (e) $\chi_{c0}(1)$, $\vec{p} = (000)$, (f) $\chi_{c0}(1)$, $\vec{p} = (100)$, (g) $\chi_{c1}(\gamma_k \gamma_5)$, $\vec{p} = (000)$, (h) $h_c(\gamma_k \gamma_4)$, $\vec{p} = (000)$

Γ	J^{PC}		$m^{(0)}/\text{MeV}$	$m^{(1)}/\text{MeV}$
γ^5	0^{-+}	η_c	2819(4)	3621(17)
γ^k	1^{--}	ψ	2916(4)	3810(22)
1	0^{++}	χ_{c0}	3287(14)	4168(52)
$\gamma^5 \gamma^k$	1^{++}	χ_{c1}	3401(28)	-
$\epsilon_{ijk} \gamma^i \gamma^j$	1^{+-}	h_c	3374(35)	-

TABLE I: Local interpolating fields, $\bar{\psi}\Gamma\psi$ and extracted charmonium spectrum, using the determination of the lattice spacing as described in the text.

The ground state masses extracted are observed to be systematically around 5% lighter than the experimental masses - this is a result of imperfect tuning of the quark mass parameter; for this first study of radiative transitions we did not attempt a more accurate tuning.

We extract a $J/\psi - \eta_c$ hyperfine splitting of 97(6)MeV. This is probably 10% larger than it would be if we had correctly tuned the quark mass, assuming the hyperfine splitting scales like m_c^{-2} ; with this correction we are in rather good agreement with the result 88(4)MeV from the closely related overlap fermion action on an isotropic lattice at Wilson $\beta = 6.3$ [20]. These two results are significantly larger than typical results using other improved actions such as clover. Assuming that there is very little change in scaling to the continuum this leaves a deviation from experiment of $\sim 30\text{MeV}$, which is consistent with the sort of deviations suggested by unquenching[17, 21] and inclusion of disconnected diagrams[22, 23].

The excited state masses we are able to extract are clearly too large in comparison with experiment. The same effect was observed in the anisotropic clover study of [24] when they set their scale using r_0 , and to a lesser extent in the studies of [16] and [25]. One possible explanation may be that, as discussed above, several excited states are contributing at intermediate times and that our fitting is not able to fully resolve them such that we end up with one effective excited state “mocking up” the effect of several². Including a second excited state into the fit hypothesis did not produce stable fits.

The multi-correlator fits were performed on the data with many \vec{p} to determine the dispersion relation for our meson states. This is particularly relevant on an anisotropic lattice where parameters in the fermion action must be tuned to match the gauge sector anisotropy and set the speed of light $c^2 \equiv \frac{E^2(\vec{p}) - m^2}{\vec{p}^2}$ equal to one. The results are shown in figure 3 where we observe that our tuning was good to the 3% level on $c = 1.032(9)$.

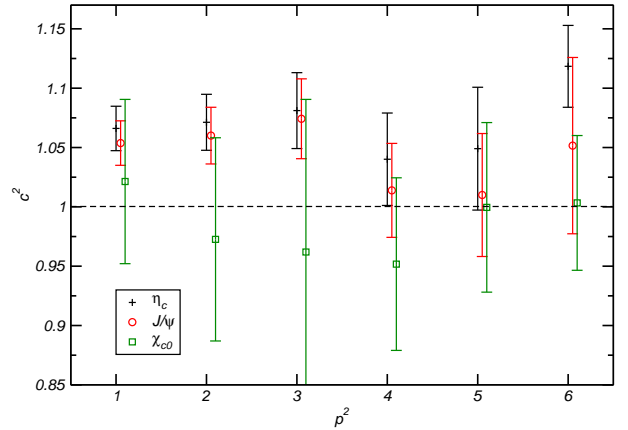


FIG. 3: Speed of light extracted from meson dispersion relation: $c^2 \equiv \frac{E^2(\vec{p}) - m^2}{\vec{p}^2}$

² Consider in particular the vector channel where the second excited state $\psi(3770)$ is very near to the first $\psi(3686)$, although its 3D_1 nature may lead to a reduced overlap with the local interpolating field

A. Charmonium decay constants

Apart from the hyperfine splitting, the only other quantities we consider that might be significantly distorted by the quenched approximation are decay constants, which are related to the meson wavefunction at the origin and are hence sensitive to short-distance physics. We discussed above that since we set the scale using long-distance dominated quantities, we expect distortion of short-distance quantities owing to the incorrect running of the QCD coupling. To be specific, the quenched coupling at short distances is too small and as such we expect the wavefunction at the origin to be depleted and hence the decay constants to be too small with respect to experiment.

We define the η_c and ψ decay constants via³

$$\begin{aligned} \langle 0|A^\mu|\eta_c(\vec{q})\rangle &= \langle 0|\bar{\psi}(0)\gamma^\mu\gamma^5\psi(0)|\eta_c(\vec{q})\rangle = if_{\eta_c}q^\mu \\ \langle 0|V^\mu|\psi(\vec{q})\rangle &= \langle 0|\bar{\psi}(0)\gamma^\mu\psi(0)|\psi(\vec{q},\lambda)\rangle = m_\psi f_\psi \epsilon^\mu(\vec{q},\lambda). \end{aligned} \quad (5)$$

In the pseudoscalar ($P = \bar{\psi}\gamma^5\psi$) case we can form the following object

$$\tilde{f}_{\eta_c} \equiv \frac{2Z_A \sum_{\vec{x}} \langle P_\sigma(\vec{x},t)A^0 \rangle}{Z_\sigma^{(0)}(e^{-m^{(0)}t} - e^{-m^{(0)}(48-t)})},$$

where the subscript σ indicates that the interpolating field is smeared with radius σ and where the superscript (0) indicates the ground state. The renormalisation of the local axial current, Z_A , will be discussed in the next section. Using (5), \tilde{f}_{η_c} is equal to

$$f_{\eta_c^{(0)}} + f_{\eta_c^{(1)}} \frac{Z_\sigma^{(1)}}{Z_\sigma^{(0)}} \frac{e^{-m^{(1)}t} - e^{-m^{(1)}(48-t)}}{e^{-m^{(0)}t} - e^{-m^{(0)}(48-t)}} + \dots \quad (6)$$

We fit the lattice data over the range $t = 9 - 22$ with this form using the $Z_\sigma^{(0,1)}$, $m^{(0,1)}$ found in the earlier two-point function fits and considering $f_{\eta_c^{(0,1)}}$ to be free fit parameters - the result for the smearing choice $\sigma = 3.6$ is shown in figure 4(a).

We can perform an analogous fit to the vector two-point data,

$$\begin{aligned} \tilde{f}_{J/\psi} &\equiv \frac{2Z_V \sum_{\vec{x}} \sum_i \langle V_\sigma^i(\vec{x},t)V^i \rangle}{3Z_\sigma^{(0)}(e^{-m^{(0)}t} + e^{-m^{(0)}(48-t)})} \\ &= f_{\psi^{(0)}} + f_{\psi^{(1)}} \frac{Z_\sigma^{(1)}}{Z_\sigma^{(0)}} \frac{e^{-m^{(1)}t} + e^{-m^{(1)}(48-t)}}{e^{-m^{(0)}t} + e^{-m^{(0)}(48-t)}} + \dots \end{aligned} \quad (7)$$

the resulting fit with $\sigma = 3.6$ being shown in figure 4(b). The renormalisation of the local vector current, Z_V is discussed in the next section.

Experimentally, the vector decay constants can be extracted from the leptonic decay widths⁴,

$$\Gamma(\psi \rightarrow e^+e^-) = \frac{4\pi}{3} \frac{4}{9} \alpha^2 \frac{f_\psi^2}{m_\psi},$$

so that, using the PDG averages[3] we have $f_{J/\psi} = 411(7)\text{MeV}$ and $f_{\psi'} = 279(8)\text{MeV}$. The η_c decay constants are rather more difficult to measure; the only result available comes from $B \rightarrow \eta_c K$ [27] and involves using a factorisation approximation to yield $f_{\eta_c} = 335(75)\text{MeV}$. It is clear that within errors $f_{J/\psi} \approx f_{\eta_c}$ as one would expect from the non-relativistic quark model in which the J/ψ and the η_c differ only by v/c suppressed spin-dependent terms.

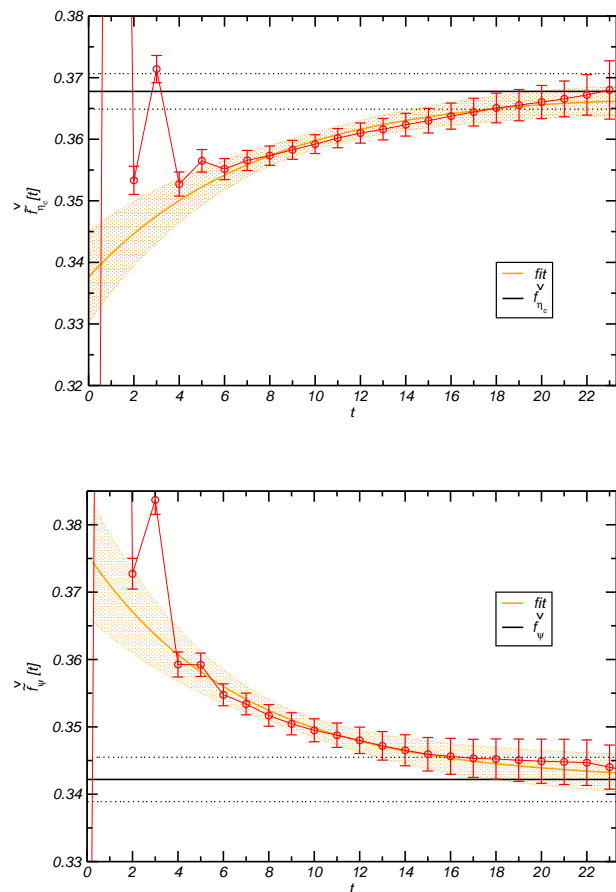


FIG. 4: Data points and fits ($t = 9 - 22$) - see equations (6), (7). The black line indicates the ground state contribution, $f^{(0)}$. Upper plot - η_c , lower plot - ψ .

³ An alternative definition for the vector decay constant is often used in lattice simulations

⁴ Note that we do not include the explicit ‘‘QCD correction’’ factor $(1 - \frac{16}{3\pi}\alpha_s)$ [26] under the assumption that all gluon effects, even hard gluons close to the charm quark mass scale, are included in the path integral computed

From our fits we extract (the scale setting on an anisotropic lattice is discussed in appendix C)

$$\begin{aligned} |f_{J/\psi}| &= 399(4)\text{MeV}; & |f_{\eta_c}| &= 429(4)(25)\text{MeV} \\ |f_{\psi'}| &= 143(81)\text{MeV}; & |f_{\eta'_c}| &= 56(21)(3)\text{MeV} \end{aligned}$$

The first error is statistical and the second, estimated systematic error, is of order 5% and accounts for the small violations of $Z_V = Z_A$ we find for our domain-wall fermions, see the following section for details.

The ground state values are in reasonable agreement with the experimental extractions, perhaps indicating that even here, with a short-distance dominated quantity, the quenched approximation is only impacting at the few percent level. It is important however to recall that our charm quark mass is a little small, and it is possible that the discrepancy caused by this is approximately canceling the quenching discrepancy. A further calculation with a slightly larger quark mass would allow for an interpolation to the true charm quark mass and a more precise estimation; since our primary interest is with radiative transitions, this additional computation has not yet been carried out.

The excited state decay constants extracted are somewhat smaller than one might expect, however we recall that we were not very successful in extracting the experimental masses for these states from two-point functions. It is possible that the excited state exponential is absorbing the effect of several excited states - a more systematic study of interpolating fields with the intent of isolating a field with large overlap on to the first excited state would clarify the issue.

IV. THREE-POINT FUNCTIONS

The field theoretic quantity that most simply encodes radiative transitions is the three-point function:

$$\begin{aligned} \Gamma_{f\Gamma_i}^{(3)}(\vec{p}_f, \vec{q}; t_f, t) \\ = \sum_{\vec{x}, \vec{y}} e^{-i\vec{p}_f \cdot \vec{x}} e^{+i\vec{q} \cdot \vec{y}} \langle O_f(\vec{x}, t_f) \bar{\psi} \Gamma \psi(\vec{y}, t) O_i^\dagger(\vec{0}, 0) \rangle \end{aligned} \quad (8)$$

The $O_{i,f}$ are interpolating fields chosen to have some overlap with whatever meson states we are interested in. The current insertion, $\bar{\psi} \Gamma \psi$, in our case is chosen to have vector quantum numbers so as to attach to an external photon. If we opt to use fermion bilinears for the meson interpolating fields, the possible Wick contractions fall into three classes:

- (a) the connected diagram of figure 5(a);
- (b) disconnected diagrams where an intermediate state without charm quarks appears, e.g. figure 5(b);
- (c) diagrams in which the photon couples to a closed fermion loop, e.g. figure 5(c).

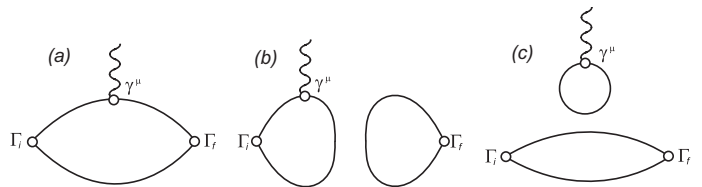


FIG. 5: Wick contractions for charmonium three-point functions. (a) connected, (b) OZI-suppressed, (c) disconnected loop

Disconnected diagrams of the type in figure 5(b) should be small - in charmonium, OZI suppression is believed to be strong, which has at least a partial explanation in QCD perturbation theory since there the intermediate two or three gluon state is suppressed as a power of $\alpha_s(\mu \sim m_c)$. We do not calculate diagrams of this type in the current computation.

Diagrams with the photon coupling to a closed fermion loop, as in figure 5(c), are zero in the case of form-factors ($i = f$), on the basis of charge-conjugation invariance of the QCD action[28]. In the case of transitions ($i \neq f$), while the “ C -odd” connected two-point function vanishes in the ensemble average, the inclusion of the “ C -odd” disconnected loop acts to compensate leaving a non-zero quantity. In the light quark sector such a diagram would be required to allow ω or ϕ VMD-style processes, although such disconnected contributions to the QCD vector correlator two-point functions are believed small as evinced by the small empirical $\omega - \phi$ mixing, and hence are unlikely to contribute much to the transitions under study. In addition, in the particular case that the vector current is electromagnetic, we also have a suppression of this disconnected contribution owing to the sum of u, d, s -quark charges being zero and there being an approximate $SU(3)$ flavour symmetry. In our quenched charmonium calculation we might consider allowing a charm-quark loop, but we expect the contribution to be small dynamically owing to the large charm quark mass and we do not explicitly include it in our computation.

We are left with the connected diagrams, figure 5(a), with the possibility of light quark loops removed since we are working in the quenched approximation. We compute these diagrams on the lattice using the sequential source technique[29]. This is simply a lattice technology that enables computation of the required propagators with only two inversions of the Dirac matrix and without computing an all-to-all propagator. The connected three-point function written in terms of fermion propagators $G_{ij}^{\alpha\beta}(x, y) = \psi_i^\alpha(x) \bar{\psi}_j^\beta(y)$ is

$$\begin{aligned} \Gamma_{f\Gamma_i}^{(3)}(\vec{p}_f, \vec{q}; t_f, t) \\ = - \sum_{\vec{x}, \vec{y}} e^{-i\vec{p}_f \cdot \vec{x}} e^{+i\vec{q} \cdot \vec{y}} \text{tr} \left\langle G(0, x) \Gamma_f G(x, y) \Gamma G(y, 0) \Gamma_i \right\rangle. \end{aligned}$$

In the sequential source technique, this is factorised as

$$\Gamma_{f\Gamma_i}^{(3)}(\vec{p}_f, \vec{q}; t_f, t) = - \sum_{\vec{y}} e^{+i\vec{q}\cdot\vec{y}} \text{tr} \left\langle \gamma_5 H_{\Gamma_f}^\dagger(y, 0; t_f; \vec{p}_f) \gamma_5 \Gamma G(y, 0) \Gamma_i \gamma_5 \right\rangle,$$

with

$$H_{\Gamma_f}(y, 0; t_f; \vec{p}_f) \equiv \sum_{\vec{x}} e^{i\vec{p}_f \cdot \vec{x}} G(y, x) \gamma_5 \Gamma_f^\dagger \gamma_5 G(x, 0) \gamma_5.$$

If the propagator $G(y, 0)$ is computed via an inversion of the Dirac matrix, $M_{\alpha\gamma}^{ik}(x, z) G_{\gamma\beta}^{kj}(z, y) = \delta_{ij} \delta_{\alpha\beta} \delta_{xy}$, then one can obtain $H_{\Gamma_f}(y, 0; t_f; \vec{p}_f)$ via one further inversion using $G(y, 0)$ in the inversion source,

$$M(z, y) H_{\Gamma_f}(y, 0; t_f; \vec{p}_f) = \delta_{t_z, t_f} e^{i\vec{p}_f \cdot \vec{z}} \gamma_5 \Gamma_f^\dagger \gamma_5 G(z, 0) \gamma_5.$$

$$\Gamma_{f\Gamma_i}^{(3)}(\vec{p}_f, \vec{q}; t_f, t) = \sum_{f,i} \frac{e^{-E_f t_f} e^{-(E_i - E_f)t}}{2E_f(\vec{p}_f) 2E_i(\vec{p}_i)} \langle 0 | \bar{\psi} \Gamma_f \psi(\vec{0}, 0) | f(\vec{p}_f, r_f) \rangle \langle f(\vec{p}_f, r_f) | \bar{\psi} \Gamma \psi(\vec{0}, 0) | i(\vec{p}_i, r_i) \rangle \left(\langle 0 | \bar{\psi} \Gamma_i \psi(\vec{0}, 0) | i(\vec{p}_i, r_i) \rangle \right)^*,$$

so that (in Euclidean space) we have a sum of decaying exponentials. If t is sufficiently far from 0 and t_f the excited state contributions should have decayed away leaving us with only the ground state transition matrix element. The removal of the excited state contributions is assisted by using the interpolating field smearing choices we made to improve plateaux in the two-point functions.

In our computation we place the source at $t = 0$ and the sink at $t = 24$ and consider insertions of the vector current on all time-slices. Since we have an antiperiodic lattice of length 48, this makes the second half of the lattice symmetric with the first and in practice we average the two halves to get our form-factor results, thus improving the statistics.

The energies of meson states and the overlap of the interpolating fields with given states (Z) are extracted from the meson two-point functions as described in section III. This allows us to adopt a fitting method for extraction of matrix elements from the three-point functions. The procedure involves writing the three-point function on a given time-slice as the sum of products of a (known) propagation factor $P = \frac{Z_f Z_i}{4E_f E_i} e^{-E_f t_f} e^{-(E_i - E_f)t}$, a (known) kinematic factor (e.g. $K^\mu = (p_f + p_i)^\mu$ for the $\eta_c \gamma^\mu \eta_c$ case) and an unknown form-factor, i.e.

$$\Gamma(p_f, p_i; t) = \sum_n P(p_f, p_i; t) \cdot K_n(p_f, p_i) \cdot f_n(Q^2).$$

One can then form a vector of three-point functions that all have the same $Q^2 = |\vec{p}_f - \vec{p}_i|^2 - (E_f - E_i)^2$ (i.e. rotationally equivalent momentum combinations and different combinations of Lorentz indices, labeled here by

The cost is that we have specified the momentum and species of the sink particle and thus we must perform a new calculation for each new particle or momentum. For this reason we performed simulations only with $\vec{p}_f = (000)$ and (100) . We are able, however, in this formalism to insert any current, Γ , with any momentum, \vec{q} . Our particular interest is with the vector insertions $\Gamma = \gamma^\mu$. In addition, we can insert any meson source gamma matrix structure Γ_i without further inversions.

The three-point function can be related to meson matrix elements of the vector current by inserting complete sets of states into (8) yielding

$a, b, c \dots$) and a matrix with entries PK , to define a linear system

$$\begin{bmatrix} \Gamma(a; t) \\ \Gamma(b; t) \\ \Gamma(c; t) \\ \vdots \end{bmatrix} = \begin{bmatrix} P(a; t)K_1(a) & P(a; t)K_2(a) & \dots \\ P(b; t)K_1(b) & P(b; t)K_2(b) & \\ P(c; t)K_1(c) & P(c; t)K_2(c) & \\ \vdots & & \ddots \end{bmatrix} \begin{bmatrix} f_1(Q^2)[t] \\ f_2(Q^2)[t] \\ \vdots \end{bmatrix},$$

which we can invert with SVD to find the form-factors $f_n(Q^2)[t]$.

Single elimination jackknife is implemented such that statistical errors are propagated through the inversion process. This proceeds by eliminating one configuration and averaging the remaining three-point function ensemble for use in the right-hand-side above and computing the propagation and kinematic factors using the equivalent “single-elimination bin” from the Z, E ensemble extracted from the two-point function fits. The SVD inversion is then performed for this “single-elimination bin”. This is repeated for elimination of each configuration yielding a configuration ensemble of solutions $\{f_n\}$.

The form-factors $f_n(Q^2)[t]$ should have no t dependence once excited states have decayed away - i.e. they have plateaux. This linear inversion formalism can also include excited state contributions explicitly, provided their energies and Z 's have been extracted from the two-point functions - we would simply enlarge the space of the linear system. In the present analysis we consider only ground state contributions - our poor estimation of the mass of excited states leads us to suspect that we are not able to isolate purely the first excited state. In

a few cases we will find that an $f_n(Q^2)[t]$ does not reach a plateau within the available time, in such cases we fit in a region around $t = 12$ (away from the domain-wall oscillations near $t = 0, 24$), with a form

$$f_n(Q^2)[t] = f_n(Q^2) + f_i e^{-m_i t} + f_f e^{-m_f(24-t)}, \quad (9)$$

with $f_n(Q^2), f_i, f_f, m_i, m_f$ as variables. A typical result of this fitting is shown in figure 6(b). Our lack of control over the contribution of excited states is demonstrated by the extracted masses, $m_{i,f}$, which are typically considerably larger than expected on the basis of either the true or our lattice first excited state masses. These fits are rather successful, suggesting that the single exponential pollution hypothesis is reasonable even though we expect contributions from several excited states - a possible explanation might arise if alternating excited state contributions oscillated in sign (either from the Z -factors or from the excited state transition matrix elements)[30]. In the following sections, $f(Q^2)$ points extracted in this manner are displayed in figures by ghosted shapes while points with a clear plateau appear with solid lines.

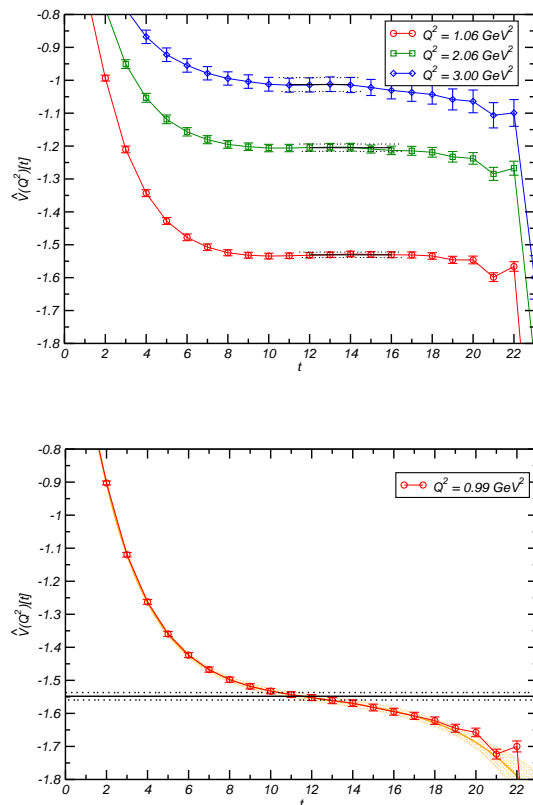


FIG. 6: Examples taken from $J/\psi \rightarrow \eta_c \gamma$ (a) plateau fits (b) fit by the function (9), parameters are $\hat{V}(Q^2) = -1.55(1)$, $f_i = 1.45(3)$, $f_f = -0.42(14)$, $m_i = 0.41(1)$, $m_f = 0.27(7)$

A possible explanation for the large values of m_i we observe comes from an alternate time-ordering allowed

by our anti-periodic lattice. The periodicity implies that there is an image of the sink at $t = -24$, such that with the “current” insertion at timeslice $t > 0$ there is a process: creation of sink particle with Γ_f at $t = -24$, insertion of a “current” Γ_i at $t = 0$ and annihilation of a vector particle by γ^μ at t . This process has time dependence $e^{-24E_f} e^{-E_\psi(\vec{q})t}$, which would correspond in the $\psi - \eta_c$ case to $m_i = E_\psi(\vec{q}) \sim 0.5$ in lattice units. A limited computation of three-point functions with Dirichlet boundary conditions appears to confirm this hypothesis.

In practice we can access a number of Q^2 values through projecting various momenta at the sink and the insertion. At the sink we are limited by the sequential source technique and only use $\vec{p}_f = (000), (100)$, but at the insertion we project many momenta, corresponding to \vec{p}_i up to around (211). Higher momenta were calculated but the signals were increasingly noisy. We used smearing at both source and sink with $\sigma = 3.6$.

A. Current renormalisation

We utilise the simple local vector current, $\bar{\psi}(x)\gamma^\mu\psi(x)$, which is not conserved with a discretised fermion action and as such gets multiplicatively renormalised by a factor $Z_V(a)$. We extract Z_V using a ratio of two-point and three-point functions evaluated at $Q^2 = 0$, which in the case of a temporal vector current is not polluted by excited state transitions[31]. For the η_c and the χ_{c0} we use

$$Z_V^{(\mu)}(t) = \frac{p^\mu}{E(\vec{p})} \frac{\frac{1}{2} \Gamma_{\eta_c \eta_c}^{(2)}(\vec{p}; t_f = 24)}{\Gamma_{\eta_c \gamma^\mu \eta_c}^{(3)}(\vec{p}_f = \vec{p}_i = \vec{p}; t_f = 24, t)}$$

where the factor of $\frac{1}{2}$ accounts for the equal contribution to the two-point function of the source at timeslice 0 and the image of the source at timeslice 48 (recall that we have a temporally anti-periodic lattice). For the spin-1 particles ($J/\psi, \chi_{c1}, h_c$) we use

$$Z_V^{(\mu)}(t) = \frac{p^\mu}{E(\vec{p})} \frac{\frac{1}{2} \sum_k \Gamma_{\psi_k \psi_k}^{(2)}(\vec{p}; t_f = 24)}{\sum_k \Gamma_{\psi_k \gamma^\mu \psi_k}^{(3)}(\vec{p}_f = \vec{p}_i = \vec{p}; t_f = 24, t)}$$

Since we are working on an anisotropic lattice the renormalisation of the spatial and temporal components of the vector current could, in principle, differ. The extracted Z_V are shown in figure 7 where it is clear that there is no significant dependence upon the particle used in the extraction. The η_c extraction is cleanest and gives:

$$Z_V^{(0)} = 1.1803(2); \quad Z_V^{(k)} = 1.130(13).$$

Note that these numbers differ by a factor comparable to the c values extracted in the dispersion relation analysis, indicating that wherever a three-momentum \vec{p} appears we should in fact insert an explicit $c = 1.032$ to account for the imperfect dispersion. In what follows we

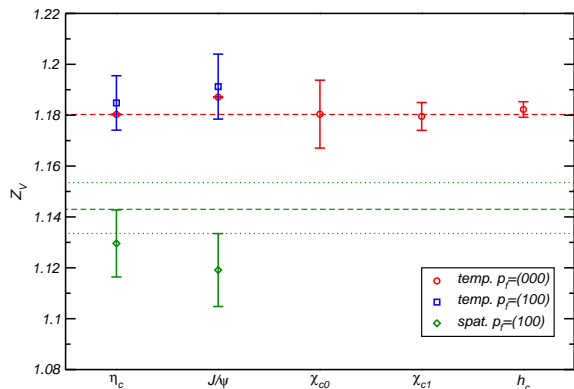


FIG. 7: Z_V extracted from two-point/three-point function ratios. Green dashed line shows $Z_V^{(0)}/c$. The extracted spatial data are obviously compatible with this.

will adopt this prescription for the momentum and use the temporal Z_V .

The renormalization factor, Z_A , for the four dimensional axial current operator $A_\mu = \bar{\psi}\gamma_\mu\gamma_5\psi$ is calculated using the five dimensional conserved axial current for domain wall fermions \mathcal{A}_μ by the relation [32] $\langle \mathcal{A}_\mu(t)A_\mu(0) \rangle = Z_A \langle A_\mu(t)A_\mu(0) \rangle$. In the limit of $L_5 \rightarrow \infty$, $Z_V = Z_A$. However, at finite L_5 there is a breaking of chiral symmetry that is characterized by a additive (and positive) quark mass shift called the residual mass m_{res} . The difference of Z_V from Z_A is proportional to this residual mass. The latter we find to be consistent with isotropic Wilson gauge calculations at the same spatial lattice spacing [32].

V. CHARMONIUM VECTOR FORM-FACTORS

Charmonia, unlike charged or flavoured mesons, do not have radiative form-factors owing to them being eigenstates of charge-conjugation invariance. At the quark level this comes about through the photon coupling to both the quark and the anti-quark with equal strength. In our lattice computation we insert the vector current only on the quark line and are thus able to access its distribution within the meson. This can be compared to models.

A. η_c “form-factor”

This is defined by the matrix element decomposition

$$\langle \eta_c(\vec{p}_f) | j^\mu(0) | \eta_c(\vec{p}_i) \rangle = f(Q^2)(p_i + p_f)^\mu. \quad (10)$$

In figure 8(a) we display some typical $f(Q^2)[t]$ as extracted from our simulation in the manner described in the previous section. We see clear plateau behaviour away from the source and sink points which is fitted and a value of $f(Q^2)$ obtained. These points are displayed in

figure 8(b). Also shown is the expectation of VMD using the J/ψ mass found in section III, this is seen to give a very poor description of the data in contrast to what is found in the light-quark sector for the pion form-factor [29]. This is to be expected on the basis of a dispersion equation approach - in the light quark sector, the ρ pole is the nearest left-hand vector singularity in the complex Q^2 plane and the next nearest (neglecting multi-pion cuts and isospin suppressed poles) is the excited $\rho'(1450)$ which is relatively distant. In charmonium the nearest pole is the $J/\psi(3097)$ and the next nearest the $\psi'(3686)$ which is not sufficiently distant as to be negligible. Hence in charmonium it is likely that one needs to sum many vector meson poles (of unknown residue) to agree with $Q^2 > 0$ data.

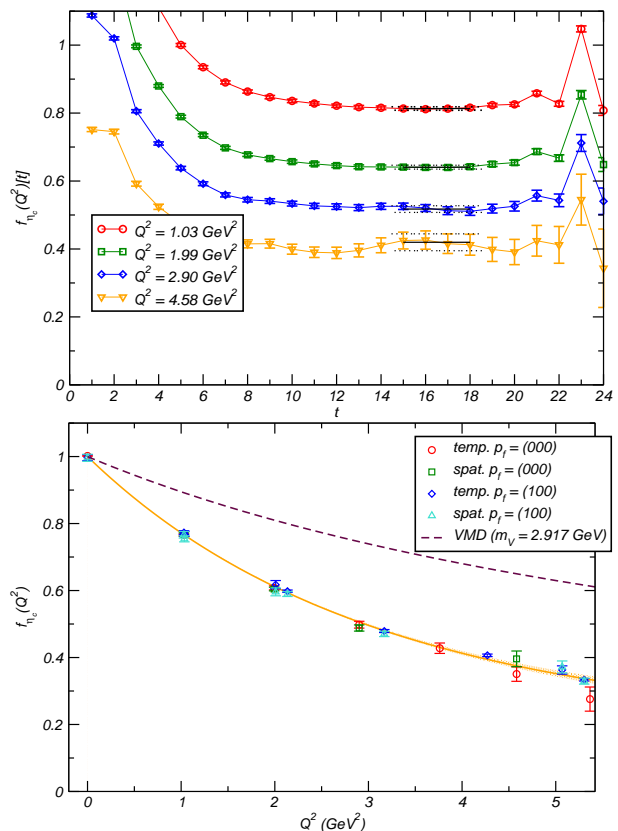


FIG. 8: η_c form-factor (a) typical lattice signal with plateau fits (b) form-factor

We take the more pragmatic approach of fitting the ($Q^2 > 0$) data to a simple analytic form, $\exp\left[-\frac{Q^2}{16\beta^2}(1 + \alpha Q^2)\right]$. This fit is also shown in figure 8(b) where one can see it faithfully reproduces the data over the entire Q^2 range considered. The fit parameters so obtained are

$$\beta = 480(3)\text{MeV}; \quad \alpha = -0.046(1)\text{GeV}^{-2}.$$

One can define a squared “charge” radius by $\langle r^2 \rangle = -6\frac{d}{dQ^2}f(Q^2)|_{Q^2=0} = \frac{6}{16\beta^2}$, which yields $\sqrt{\langle r^2 \rangle} =$

0.255(2)fm, giving some a posteriori justification for our lattice size being only ~ 1.2 fm.

As mentioned in the introduction, most charmonium phenomenology is done within the framework of quark-potential models. These models are usually of the non-relativistic Schrödinger equation type, utilising some phenomenologically justified static potential and incorporating relativistic corrections to this, such as spin-spin and spin-orbit terms. By and large these models are successful so it makes sense for us to compare our lattice results with them in cases where there is not experimental data.

In the simplest forms of these models we have only Galilean invariance and not the full Lorentz invariance of a relativistic theory. This is manifested in the factorisation of the spatial wavefunction of a charmonium state into centre-of-mass and internal wavefunctions:

$$|\eta_c(\vec{p})\rangle \propto \int d^3\vec{R} e^{i\vec{p}\cdot\vec{R}} \int d^3\vec{r} \psi(\vec{r}),$$

with $\psi(\vec{r})$ independent of the η_c momentum \vec{p} , obtained by solving a Schrödinger equation in the rest frame of the η_c . This poses problems of frame-dependence when one calculates matrix elements. Consider calculating $f(Q^2)$ using equation (10) within this model. We want to work in a frame near to the one in which the η_c wavefunction was calculated, to minimise the neglected boost effects, two choices strike us:

- *the rest frame of the initial η_c* ($\vec{p}_i = 0, \vec{p}_f = \vec{q}$). Here only the end-state η_c could suffer boost distortion. We have

$$f(Q^2 = 2m_{\eta_c}^2 [-1 + (1 + \frac{|\vec{q}|^2}{m_{\eta_c}^2})^{1/2}]) \propto \int d^3\vec{r} \psi^*(\vec{r}) j_0(\frac{|\vec{q}|r}{2}) \psi(\vec{r})$$

With approximate harmonic oscillator wavefunctions ($\psi(\vec{r}) \propto e^{-\beta^2 r^2}$) we obtain

$$f_{\text{RF}}(Q^2) \rightarrow \exp\left[-\frac{|\vec{q}|^2}{16\beta^2}\right] = \exp\left[-\frac{Q^2}{16\beta^2}\left(1 + \frac{Q^2}{4m_{\eta_c}^2}\right)\right]$$

- *the Breit frame* ($\vec{p}_i = -\frac{\vec{q}}{2}, \vec{p}_f = \frac{\vec{q}}{2}$). Here we share the possible boost distortion equally between the initial and final states. The quark-model evaluation

of the matrix element will be essentially identical to the previous case with the only difference being that now $Q^2 = |\vec{q}|^2$. Hence

$$f_{\text{BF}}(Q^2) \rightarrow \exp\left[-\frac{|\vec{q}|^2}{16\beta^2}\right] = \exp\left[-\frac{Q^2}{16\beta^2}\right]$$

and we explicitly see the frame-dependence of the simplest quark models ($f_{\text{BF}}(Q^2) \neq f_{\text{RF}}(Q^2)$).

If Q^2 is small, all frames will agree, and it is really only here that we have a unique quark model form. In [33], a thorough analysis of these concerns is applied to the case of the proton form-factors.

We note in passing that light-front quark models have the same sort of problems - although boosts along a given axis become simple (kinematical), which may admit consistency up to higher Q^2 , we lose rotational invariance, and this can lead to extra form-factors not present in a picture with $O(3)$ symmetry[34].

In the quark model of ISGW [35], form-factors have a dependence near $Q^2 = 0$ of the form $\exp\left[-\frac{Q^2}{16\beta^2\kappa^2}\right]$, with $\kappa \sim 0.7$. The κ factor was added by hand to better describe the pion form-factor and certain heavy quark transitions and was ascribed an origin in relativistic corrections⁵. An alternative origin might be the effect of gluonic degrees-of-freedom not considered in the simple potential model[37, 38]. In [39] a Schrödinger equation with a Coulomb plus linear potential and spin-dependent corrections was solved using a variational harmonic oscillator basis - they found for the η_c that $\beta = 710$ MeV. Hence $\kappa\beta = 500$ MeV which is in rather good agreement with our $\beta = 480(3)$ MeV, suggesting that the potential model, with the relativistic correction, is capturing at least some of the $Q^2 \approx 0$ physics we have on the lattice.

B. J/ψ “form-factors”

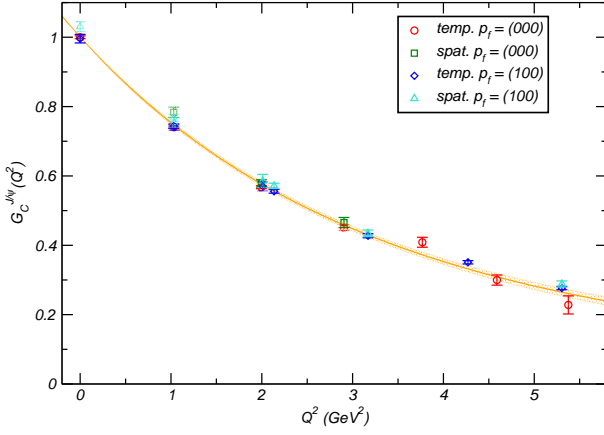
A vector particle has three form-factors, a suitable set being those of definite multipolarity: charge - $G_C(Q^2)$, magnetic dipole - $G_M(Q^2)$ and quadrupole - $G_Q(Q^2)$. These are defined in terms of the standard Lorentz covariant decomposition

$$\begin{aligned} \langle V(\vec{p}_f, r_f) | j^\mu(0) | V(\vec{p}_i, r_i) \rangle &= -(p_f + p_i)^\mu \left[G_1(Q^2) \epsilon^*(\vec{p}_f, r_f) \cdot \epsilon(\vec{p}_i, r_i) + \frac{G_3(Q^2)}{2m_\eta^2} \epsilon^*(\vec{p}_f, r_i) \cdot p_i \epsilon(\vec{p}_i, r_i) \cdot p_f \right] \\ &\quad + G_2(Q^2) \left[\epsilon^\mu(\vec{p}_i, r_i) \epsilon^*(\vec{p}_f, r_f) \cdot p_i + \epsilon^{\mu*}(\vec{p}_f, r_f) \epsilon(\vec{p}_i, r_i) \cdot p_f \right] \end{aligned}$$

by

$$\begin{aligned} G_C &= \left(1 + \frac{2}{3}\eta\right) G_1 - \frac{2}{3}\eta G_2 + \frac{2}{3}\eta(1 + \eta)G_3 \\ G_M &= -G_2 \\ G_Q &= G_1 - G_2 + (1 + \eta)G_3, \end{aligned}$$

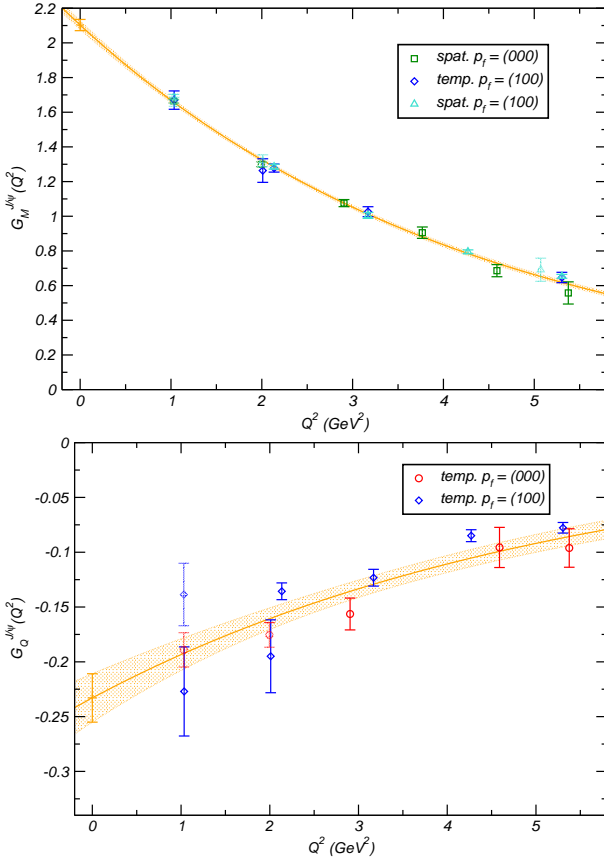
with $\eta = \frac{Q^2}{4m^2}$. In figure 9 we display our lattice points and a fit to them. The charge multipole is fitted by the same function we used for the η_c with resulting parame-

FIG. 9: J/ψ “charge” form-factor

ters:

$$\beta_C = 470(7)\text{MeV}; \quad \alpha = -0.022(7)\text{GeV}^{-2}. \quad (11)$$

This similarity of these parameters to those extracted for the η_c indicate that these two particles have spatial wavefunctions that are rather alike. The magnetic dipole and

FIG. 10: J/ψ form-factors (a) magnetic (b) quadrupole

quadrupole form-factors, displayed in figure 10, have fits

of the form $G(0) \exp -\frac{Q^2}{16\beta^2}$ which are seen to be successful and yield

$$\begin{aligned} \beta_M &= 520(8)\text{MeV}; & G_M(0) &= 2.10(3) \\ \beta_Q &= 580(44)\text{MeV}; & G_Q(0) &= -0.23(2). \end{aligned}$$

The quadrupole form-factor at $Q^2 = 0$ gives us the quadrupole moment of the J/ψ and, via a quark-model interpretation, access to the quark-antiquark D -wave admixture in the dominantly S -wave J/ψ . The quadrupole moment operator is [40] $\mathbf{Q} = r^2(3\cos^2\theta - 1) = \sqrt{\frac{16\pi}{5}}r^2Y_2^0(\theta, \phi)$. Then it is clear that $\langle S|\mathbf{Q}|S\rangle = 0$, while $\langle S|\mathbf{Q}|D\rangle \neq 0$. In the approximate harmonic oscillator basis, we have

$$\langle J/\psi|\mathbf{Q}|J/\psi\rangle = 2\sqrt{3}a_S a_D \beta^{-2},$$

where a_L is the L -wave amplitude in the J/ψ wavefunction. Since $G_Q(0) = m_{J/\psi}^2 \langle \mathbf{Q} \rangle$, using our lattice J/ψ mass we have $\langle \mathbf{Q} \rangle = -0.027(3)\text{GeV}^{-2}$. With the extracted quadrupole β_Q value, and assuming $a_S \approx 1$ we find $a_D = -2.6(5) \times 10^{-3}$. This very small value can be used to constrain the size of any tensor term one might wish to add to a charmonium model Hamiltonian. We remind the reader that any contribution from coupled-channel $D\bar{D}$ loops will not be present in our quenched computation.

The magnetic dipole moment, $\mu_{J/\psi}$, can be extracted using $G_M(0) = 2M_{J/\psi} \mu_{J/\psi}$ - in units of the J/ψ mass it is $1.05(2)$. Within the simple non-relativistic quark model this quantity can be expressed as

$$(1 + \delta) \left[(1 + \kappa_c) |a_S|^2 + \frac{1}{4}(1 - 2\kappa_c) |a_D|^2 \right],$$

where $\delta = \frac{M_{J/\psi} - 2m_c}{2m_c}$ and κ_c is the anomalous magnetic moment of the charm quark. With the D -wave admixture extracted from the quadrupole moment, the second term in square brackets is negligible. If one had a way of unambiguously setting the charm quark mass one could use this expression to extract the charm quark anomalous magnetic moment - however this is not possible even in principle - the quark mass is a renormalisation scheme dependent quantity. In quark potential models it is usually tuned along with other parameters to give a good description of the spectrum. A conservative interpretation of our extracted value would be that it could be explained in a model with a small or zero anomalous quark moment and a charm quark “mass” slightly less than half the J/ψ mass. This would be interesting application of the EFT method of pNRQCD [41]- within this picture one has, at a given order in the power counting, a relationship between the charm quark mass and the J/ψ mass in terms only of the (determined) strong coupling, as such one can determine, at the same order in the power counting, the anomalous moment κ_c .

C. χ_{c0} “form-factor”

This has the same decomposition as does the η_c , eqn (10). Our lattice three-point functions here are much noisier than for the η_c and J/ψ , but there are sufficiently clear plateaux to extract the values plotted in figure 11.

The data is fitted with the form $f(0)e^{-\frac{Q^2}{16\beta^2}}$ giving $f(0) = 1.0015(15)$, consistent with 1 as it should be, and $\beta = 393(12)\text{MeV}$, which is roughly consistent with the quark model value[39] $\kappa\beta = 340\text{MeV}$. That this is smaller than the $\eta_c, J/\psi$ β is simply a reflection of the fact that the χ_{c0} is spatially larger due to the centripetal P -wave barrier between the quark and the anti-quark.

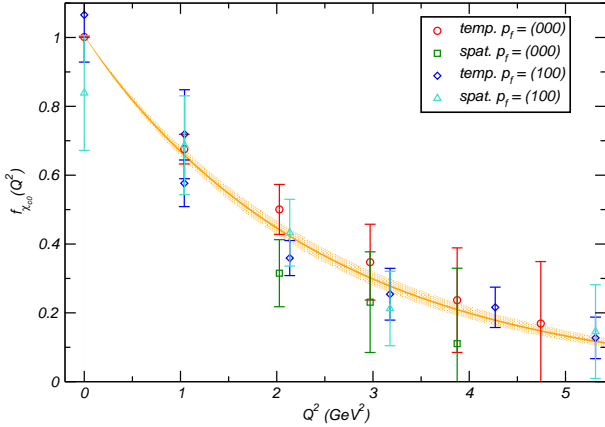


FIG. 11: χ_{c0} form-factor

VI. RADIATIVE TRANSITIONS

A. $J/\psi \rightarrow \eta_c \gamma_{M1}$

The Minkowski space-time matrix element for this transition can be expressed in terms of a product of one Lorentz invariant form-factor and one Lorentz covariant kinematic factor:

$$\langle \eta_c(\vec{p}') | j^\mu(0) | J/\psi(\vec{p}, r) \rangle = \frac{2V(Q^2)}{m_{\eta_c} + m_\psi} \epsilon^{\mu\alpha\beta\gamma} p'_\alpha p_\beta \epsilon_\gamma(\vec{p}, r). \quad (12)$$

This decomposition is parity invariant and, with $V(Q^2)$ real, time-reversal invariant. The Lorentz invariant matrix element for $J/\psi \rightarrow \eta_c \gamma^*(Q^2)$ is the contraction of (12) with a final-state photon polarization vector:

$$\mathcal{M}_{r, r_\gamma} = \epsilon_\mu^*(\vec{q}, r_\gamma) \langle \eta_c(\vec{p}') | j^\mu(0) | J/\psi(\vec{p}, r) \rangle.$$

The decay width with an on-shell photon is

$$\Gamma(J/\psi \rightarrow \eta_c \gamma) = \int d\Omega_{\hat{q}} \frac{1}{32\pi^2} \frac{|\vec{q}|}{m_\psi^2} \frac{1}{3} \sum_{r, r_\gamma} |\mathcal{M}_{r, r_\gamma}|^2, \quad (13)$$

which contains a sum over the final state photon polarisation and an average over the initial ψ polarisation. Explicitly then we have

$$\Gamma(J/\psi \rightarrow \eta_c \gamma) = \frac{1}{4\pi} \frac{|\vec{q}|^3}{(m_{\eta_c} + m_\psi)^2} \frac{4}{3} |V(0)|^2.$$

In our lattice computation we couple only to the quark and not to the anti-quark and do not include the quark electric charge factor. As such we compute $\hat{V}(Q^2)$ which is related to $V(Q^2)$ by⁶

$$V(Q^2) = 2 \times \frac{2}{3} e \times \hat{V}(Q^2),$$

and hence

$$\Gamma(J/\psi \rightarrow \eta_c \gamma) = \alpha \frac{|\vec{q}|^3}{(m_{\eta_c} + m_\psi)^2} \frac{64}{27} |\hat{V}(0)|^2. \quad (14)$$

There is only one direct experimental measurement of this width [42], $\Gamma_{\text{CB}}(J/\psi \rightarrow \eta_c \gamma) = 1.14(33)\text{keV}$. There are, in addition, several measurements of the product branching ratio for the process $J/\psi \rightarrow \eta_c \gamma \rightarrow \phi \phi \gamma$ [3] and one independent measurement of $\eta_c \rightarrow \phi \phi$ [43]. Taken together these data give $\Gamma_{\phi\phi}(J/\psi \rightarrow \eta_c \gamma) = 2.9(1.5)\text{keV}$, which is consistent within the large errors with the Crystal Ball result.

There is an essential ambiguity in how we compare our lattice results with the experimental data which arises from the fact that our lattice charmonia masses do not coincide exactly with the physical masses. The problem lies in whether we should use experimental or lattice masses in equation (14). $|\vec{q}|$ is closely related to the hyperfine splitting which is rather sensitive to details of the lattice calculation (as discussed in section III), hence we observe considerable difference in using lattice or experimental masses:

$ \hat{V}(0) _{\text{expt.}}$	Crystal Ball	“ $\phi\phi$ ”
phys. masses	1.27(19)	2.02(52)
latt. masses	1.56(22)	2.48(64)

We extract $\hat{V}(Q^2)$ from three-point functions computing using the following sequential sources at the sink: $\pi[\vec{p}_f = (0, 0, 0); (1, 0, 0)]; \rho_{(x, y, z)}[\vec{p}_f = (0, 0, 0); (1, 0, 0)]$. The values from different sink particle and momentum choices are all seen to be consistent suggesting that the sequential source technique is working correctly. The lattice data displayed in figure 12 is fitted with

$$\hat{V}(Q^2) = \hat{V}(0) e^{-\frac{Q^2}{16\beta^2}}$$

where we find

$$\hat{V}(0) = 1.85(4); \quad \beta = 540(10)\text{MeV}.$$

⁶ $\hat{V}(Q^2)$ is what would appear if we were computing the $\rho^+ \rightarrow \pi^+ \gamma$ transition in the isospin limit

This agrees reasonably with the Crystal Ball result in the case of using lattice masses throughout. Without performing a computation at the correct quark mass and relaxing approximations sufficiently to duplicate the experimental hyperfine splitting, we cannot give a more definitive result.

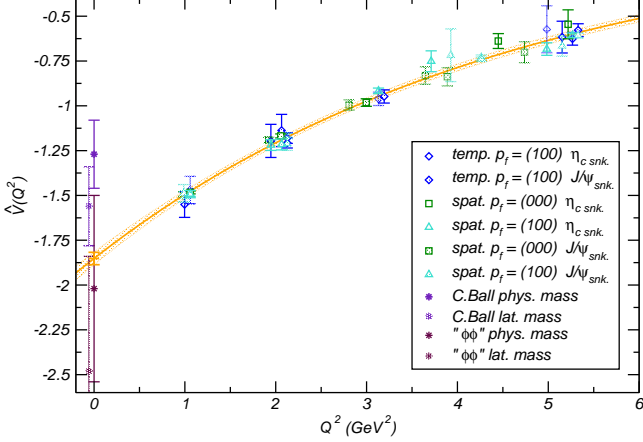


FIG. 12: $J/\psi \rightarrow \eta_c \gamma$ transition form-factor

The gaussian fit performed to the data was clearly rather successful; if we wish we can motivate such a form by returning to the sort of simple quark models considered in the previous section. Within these models one performs a non-relativistic reduction of the current operator and computes the matrix element of this between the J/ψ and η_c wavefunctions. This is a magnetic dipole (M_1) transition that occurs through quark spin-flip - the lowest order current operator (in an expansion in v/c) has the form $\vec{\sigma} \times (\vec{p}'_q - \vec{p}_q)$. Computing in any frame (recalling that the wavefunctions are assumed to be unchanged under boosts and that we have the minimal non-relativistic reduction of the current) we find

$$V(Q^2) \propto \int r^2 dr R_{\eta_c}^*(r) j_0\left(\frac{|\vec{q}|r}{2}\right) R_{\psi}(r) \rightarrow \exp\left[-\frac{|\vec{q}|^2}{16\bar{\beta}^2}\right]$$

for harmonic oscillator wavefunctions. If the η_c and J/ψ are allowed different $\bar{\beta}$ then $\bar{\beta}^2 = \frac{1}{2}(\bar{\beta}_{\eta_c}^2 + \bar{\beta}_{\psi}^2)$. Once again we encounter the problem that $V(Q^2)$ should be frame independent, but $|\vec{q}|$ is not. In the rest frame of a decaying J/ψ , a “natural” frame to consider for this process,

$$|\vec{q}|^2 = \frac{(m_{\psi}^2 - m_{\eta_c}^2)^2 + 2Q^2(m_{\psi}^2 + m_{\eta_c}^2) + Q^4}{4m_{\psi}^2}.$$

At small Q^2 , $|\vec{q}|^2 \rightarrow \frac{(m_{\psi}^2 - m_{\eta_c}^2)^2}{4m_{\psi}^2} + Q^2 \frac{1}{2} \left(1 + \frac{m_{\eta_c}^2}{m_{\psi}^2}\right)$, which means the simple quark model with harmonic oscillator wavefunctions has the same Q^2 -dependence as our fit. Other reasonable frames, in the small Q^2 limit, have the same dependence.

Performing the full calculation (with $\kappa_c = 0$) at $Q^2 = 0$ in a quark model gives an expression like [44, 45]

$$\Gamma = \alpha \frac{4e_c^2}{3m_c^2} |\vec{q}|^3 \left| \int r^2 dr R_{\eta_c}^*(r) j_0\left(\frac{|\vec{q}|r}{2}\right) R_{\psi}(r) \right|^2,$$

which can be used to evaluate the width provided the wavefunctions and the mass of the charm quark are known. Determining this latter quantity is a tricky issue - it is usually set at the Schrödinger equation stage along with the phenomenological potential parameters such that the mass spectrum is reproduced, however a unique solution is not easily found and as such this mass parameter can vary considerably between models, e.g. $m_c = 1.84\text{GeV}$ in [44] while $m_c = 1.628\text{GeV}$ in [46] and even $m_c = 1.479\text{GeV}$ in [45]. Given this uncertainty, estimates for the M_1 transitions are rather imprecise, depending as they do, on the inverse square of the mass⁷. In principle we do not have this problem in our lattice simulations - while we do vary the quark mass to get agreement with the spectrum (we have to set the charm quark mass somehow), we have no other free parameters to vary. Unfortunately, as discussed in section III we did not tune the quark mass perfectly and this is a source of some systematic error on our result for this transition and may be the reason our result is somewhat too large (recall that our quark mass is slightly too small).

B. $\chi_{c0} \rightarrow J/\psi \gamma_{E1, C1}$

Experimentally it is only possible to access transverse on-shell ($Q^2 = 0$) photons in this transition and the matrix element is purely through the electric dipole (E_1). In more generality, if we allow $Q^2 \neq 0$ and necessarily also longitudinal photons, there is a second multipole, labeled C_1 . The decomposition of the transition matrix element in terms of these multipoles is derived in the appendix and we reproduce it here:

$$\langle S(\vec{p}_S) | j^\mu(0) | V(\vec{p}_V, r) \rangle = \Omega^{-1}(Q^2) \left(E_1(Q^2) \left[\Omega(Q^2) \epsilon^\mu(\vec{p}_V, r) - \epsilon(\vec{p}_V, r) \cdot p_S (p_V^\mu p_V \cdot p_S - m_V^2 p_S^\mu) \right] + \frac{C_1(Q^2)}{\sqrt{q^2}} m_V \epsilon(\vec{p}_V, r) \cdot p_S \left[p_V \cdot p_S (p_V + p_S)^\mu - m_S^2 p_V^\mu - m_V^2 p_S^\mu \right] \right).$$

The Lorentz invariant matrix elements for the transition $\chi_{c0} \rightarrow J/\psi \gamma^*(Q^2)$ are also given in the appendix:

$$\begin{aligned} \mathcal{M}(r_\gamma = \pm; r_\psi = \mp) &= E_1(Q^2) \\ \mathcal{M}(r_\gamma = 0; r_\psi = 0) &= -C_1(Q^2). \end{aligned}$$

Hence the analogue of (13) gives for the width at $Q^2 = 0$,

$$\Gamma(\chi_{c0} \rightarrow J/\psi \gamma) = \alpha \frac{|\vec{q}|}{m_{\chi_{c0}}^2} \frac{16}{9} |\hat{E}_1(0)|^2,$$

where the lattice form-factor is again related to the physical one by $E_1(Q^2) = 2 \times \frac{2}{3} e \times \hat{E}_1(Q^2)$.

The most recent measurement of this decay's branching fraction comes from the CLEO collaboration[4], who find, using the PDG total width to normalise: $\Gamma(\chi_{c0} \rightarrow J/\psi \gamma) = 204(31)\text{keV}$. In addition to this we have the PDG[3] average/fit to data obtained up to 2005 which gives $\Gamma(\chi_{c0} \rightarrow J/\psi \gamma) = 115(14)\text{keV}$. The next PDG report will likely contain the CLEO value in a new average which will thus lie between these two values.

In figure 13 we display the $\hat{E}_1(Q^2)$ extracted from our lattice simulations. Temporal vector current insertions produce compatible results but with much larger error bars and are not shown.

Our simulation data lies at $Q^2 \neq 0$, but since we are primarily interested in the photopoint we require some fit function to allow us to extrapolate back. In the light of the success of forms motivated by the non-relativistic quark model in previous sections we consider using a function which resembles one that would be derived in such a model. We opt to use a form

$$\hat{E}_1(Q^2) = \hat{E}_1(0) \left(1 + \frac{Q^2}{\rho^2} \right) \exp \left[-\frac{Q^2}{16\beta^2} \right], \quad (15)$$

which has the gaussian behaviour used previously modified by a polynomial in Q^2 . In the simple quark model, the Q^2/ρ^2 term could arise from relativistic corrections or departures from gaussian wavefunction behaviour. Note that this form is analytic for $Q^2 > 0$ as we would expect - singularities (as in the VMD case) will occur at $Q^2 < 0$.

We do not include in the fit the points at $Q^2 < 0$ - these data, corresponding to the case $\vec{p}_f = \vec{p}_i$ where $Q^2 = -(E_f - E_i)^2$, were extracted from correlators with no plateau behaviour using the fitting method described in section IV. It is therefore a rather non-trivial cross-check that our fit function, constrained by points at $Q^2 \gtrsim$

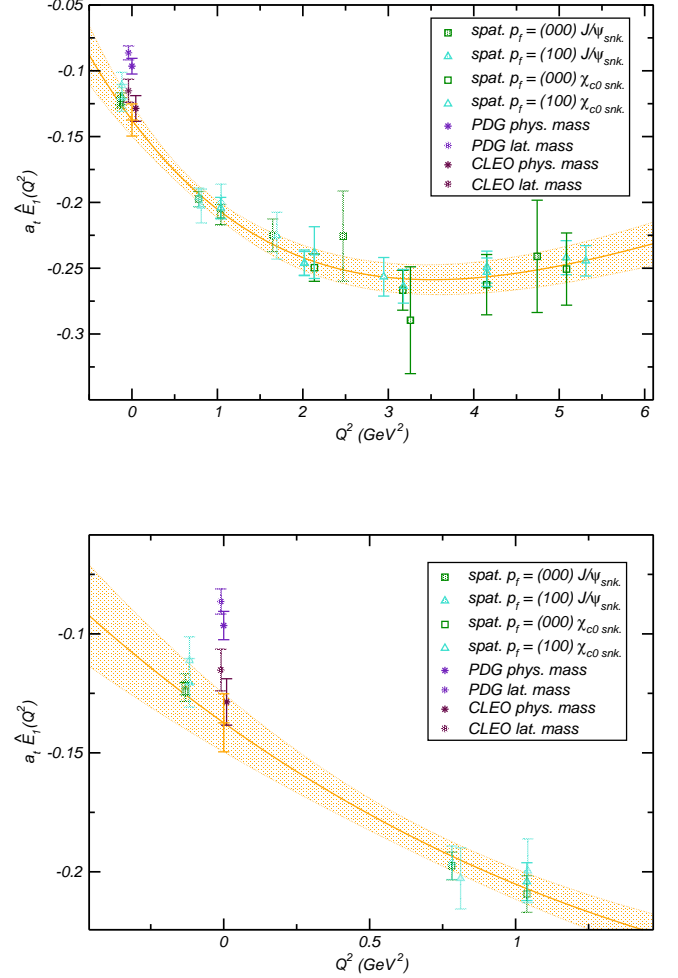


FIG. 13: $\chi_{c0} \rightarrow J/\psi \gamma$ E_1 transition form-factor. (a) full range of lattice data (b) zoom to the $Q^2 \approx 0$ region

1GeV^2 , extrapolated to the $Q^2 < 0$ region, overlays these points.

The fit returns the following parameters:

$$\begin{aligned} a_t \hat{E}_1(0) &= -0.137(12) \\ \beta &= 542(35)\text{MeV}; \quad \rho = 1.08(13)\text{GeV} \end{aligned}$$

The longitudinal photon transition form-factor, $C_1(Q^2)$ can also be extracted from lattice three-point

functions. We display our data in figure 14. As discussed in the appendix, $\frac{C_1(Q^2)}{\sqrt{q^2}}$ is real for real $Q^2 = -q^2$ if time-reversal invariance holds - thus for $Q^2 > 0$, $C_1(Q^2)$ is imaginary. The fit is to the function $i\tilde{c}\sqrt{Q^2}e^{-\frac{Q^2}{16\beta^2}}$ which has the required property that $C_1(Q^2 \rightarrow 0) \rightarrow 0$ and which is what one would expect in a simple quark model.

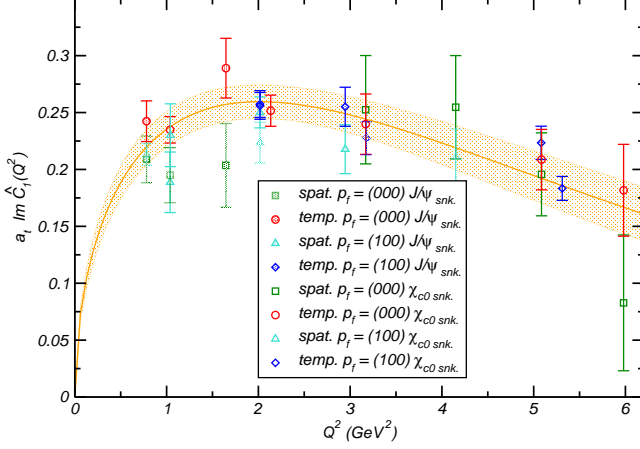


FIG. 14: $\chi_{c0} \rightarrow J/\psi\gamma$ C_1 transition form-factor

The fit suffers from the large error bars on the data, but does at least yield a β value compatible with the value extracted from the E_1 fit:

$$a_t \tilde{c} = 1.83(16); \quad \beta = 501(33)\text{MeV}$$

C. $\chi_{c1} \rightarrow J/\psi\gamma_{E1,M2,C1}$

With real photons this transition receives contributions from two multipoles, the dominant electric dipole (E_1) and a much suppressed magnetic quadrupole (M_2). Experimentally the M_2 contribution is measured through the angular distribution of photons - the PDG[3] average the two extractions performed[47, 48], each of which found a number consistent with zero, to give

$$\frac{M_2(0)}{\sqrt{E_1(0)^2 + M_2(0)^2}} = -0.002^{+0.008}_{-0.017}.$$

Appendix A contains the tools required to derive the relation connecting the transition matrix element with the multipole amplitudes:

$$\begin{aligned} \langle A(\vec{p}_A, r_A) | j^\mu(0) | V(\vec{p}_V, r_V) \rangle &= \frac{i}{4\sqrt{2}\Omega(Q^2)} \epsilon^{\mu\nu\rho\sigma} (p_A - p_V)_\sigma \times \\ &\times \left[E_1(Q^2) (p_A + p_V)_\rho \left(2m_A [\epsilon^*(\vec{p}_A, r_A) \cdot p_V] \epsilon_\nu(\vec{p}_V, r_V) + 2m_V [\epsilon(\vec{p}_V, r_V) \cdot p_A] \epsilon_\nu^*(\vec{p}_A, r_A) \right) \right. \\ &+ M_2(Q^2) (p_A + p_V)_\rho \left(2m_A [\epsilon^*(\vec{p}_A, r_A) \cdot p_V] \epsilon_\nu(\vec{p}_V, r_V) - 2m_V [\epsilon(\vec{p}_V, r_V) \cdot p_A] \epsilon_\nu^*(\vec{p}_A, r_A) \right) \\ &+ \frac{C_1(Q^2)}{\sqrt{q^2}} \left(-4\Omega(Q^2) \epsilon_\nu^*(\vec{p}_A, r_A) \epsilon_\rho(\vec{p}_V, r_V) \right. \\ &\left. \left. + (p_A + p_V)_\rho \left[(m_A^2 - m_V^2 + q^2) [\epsilon^*(\vec{p}_A, r_A) \cdot p_V] \epsilon_\nu(\vec{p}_V, r_V) + (m_A^2 - m_V^2 - q^2) [\epsilon(\vec{p}_V, r_V) \cdot p_A] \epsilon_\nu^*(\vec{p}_A, r_A) \right] \right) \right]. \end{aligned} \quad (16)$$

In extracting these amplitudes from our lattice three-point functions we are struck with the problem that our χ_{c1} signal (from the operator $\gamma^i\gamma^5$) becomes noisy after relatively few timeslices, in fact at roughly the same time that the two-point function begins to plateau (see figure 1(b,c)). Because of this it was only possible to extract a convincing signal for the χ_{c1} with $\vec{p}_f = (000)$, which considerably limits the number of three-point functions available to us for the transition $\chi_{c1} \rightarrow J/\psi\gamma$. In ad-

dition the plateaux in the few available correlators are borderline, so that for the lowest Q^2 point a fit of the form (9) was applied.

In figure 15 we show the extracted $E_1(Q^2)$ and a fit of the same form as used for $\chi_{c0} \rightarrow J/\psi\gamma_{E1}$. Within the large extrapolated error we are in agreement with the experimental data. Unfortunately, unlike in the $\chi_{c0} \rightarrow J/\psi\gamma$ case, the E_1 kinematical factor for $\vec{p}_f = \vec{p}_i$ where $Q^2 \approx 0$, is zero, so we cannot directly obtain $E_1(Q^2 \approx$

0) and the subsequent cross-check on the extrapolation which gave parameters,

$$a_t \hat{E}_1(0) = 0.312(39)$$

$$\beta = 555(113)\text{MeV}; \quad \rho = 1.65(59)\text{GeV}$$

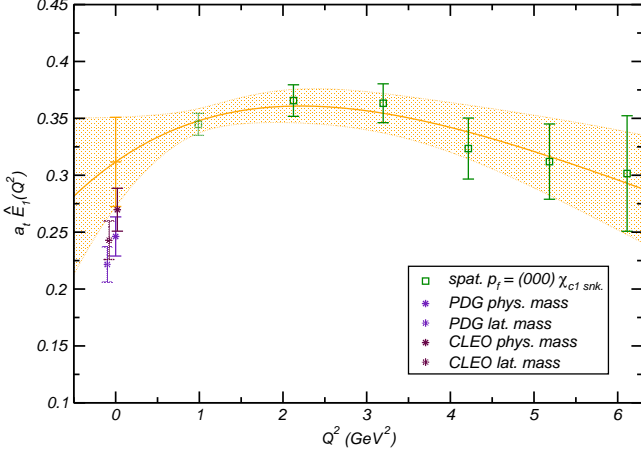


FIG. 15: $\chi_{c1} \rightarrow J/\psi\gamma$ E_1 transition form-factor

In figure 16 we show the extracted $M_2(Q^2)$. The fit has the same functional form as in the E_1 case and returns parameters:

$$a_t \hat{M}_2(0) = -0.062(37)$$

$$\beta = 617(142)\text{MeV}; \quad \rho = 0.93(47)\text{GeV}$$

The β value is compatible within the large error with the value extracted from the E_1 data.

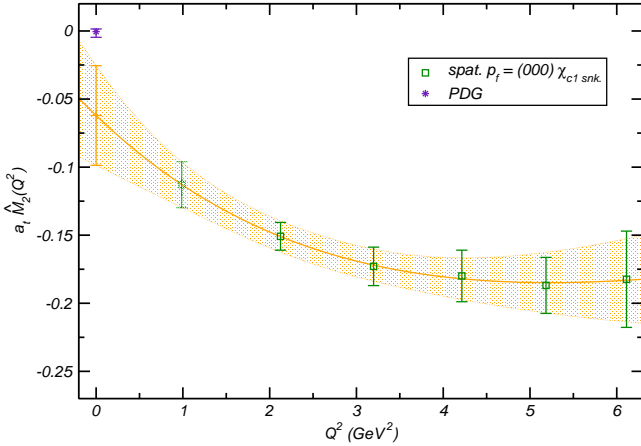


FIG. 16: $\chi_{c1} \rightarrow J/\psi\gamma$ M_2 transition form-factor

We observe in figure 16 that our lattice data extrapolates down to a value consistent with zero and hence with experiment, within large errors, at $Q^2 = 0$.

There are a number of approaches we might consider to reduce the error bar on the predicted value. The first is simply brute force; evaluate on a larger number of gauge field configurations, thus reducing the statistical fluctuations. Another option, which would also require increased computation time, is to work with a larger spatial volume (at the same lattice spacing); this allows smaller discrete three-momenta and hence access to points closer to $Q^2 = 0$, the reduced extrapolation distance then reducing the error on the extrapolated point. A third possibility, ideally combined with the previous two, is to enhance the χ_{c1} plateaux by finding an interpolating field with maximal overlap on to the ground state χ_{c1} . This might involve diagonalising a matrix of two-point functions in a basis of different smearings.

Finally we have the longitudinal photon multipole C_1 which we display in figure 17 along with a fit of same type as used for the $\chi_{c0} \rightarrow J/\psi\gamma$ transition. From the fit

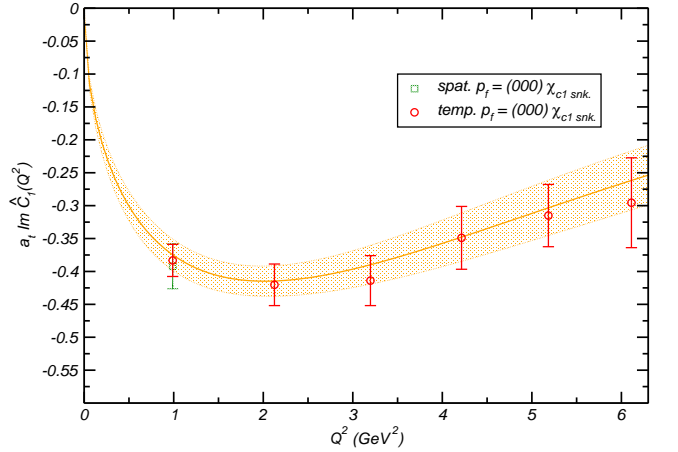


FIG. 17: $\chi_{c1} \rightarrow J/\psi\gamma$ C_1 transition form-factor

we extract

$$a_t \tilde{c} = -2.91(26); \quad \beta = 502(38)\text{MeV}$$

D. $h_c \rightarrow \eta_c \gamma_{E1, C1}$

The h_c , with $J^{PC} = 1^{+-}$, was only recently observed with high significance by the CLEO collaboration [49, 50]. The reason for the delay of discovery with respect to the other ground state charmonia lies in the difficulty of production - the process eventually utilised was the isospin violating $\psi(2S) \rightarrow \pi^0 h_c$ with a subsequent $h_c \rightarrow \eta_c \gamma$. Since only the product branching fraction $\mathcal{B}(\psi(2S) \rightarrow \pi^0 h_c) \mathcal{B}(h_c \rightarrow \eta_c \gamma)$ is measured, our calculation of $\Gamma(h_c \rightarrow \eta_c \gamma)$ constitutes a prediction.

The form-factor decomposition is identical to the $\chi_{c0} \rightarrow J/\psi\gamma$ case. Here again we suffer from poor two-point functions - we were only able to extract a convincing h_c signal in the $\vec{p}_f = (000)$ case and as such we can use only three-point functions with the h_c at rest. Despite this limitation we are able to extract some clean plateaux in a few cases and in the remaining cases we fit using (9) - we plot the extracted E_1 in figure 18. The fit shown (which is to all points including the one at $Q^2 < 0$) is of the form

$$\hat{E}_1(0) \exp -\frac{Q^2}{16\beta^2},$$

since the data does not seem to require a $\frac{Q^2}{\rho^2}$ term (ρ^{-1} in such a fit is very small). We find

$$a_t \hat{E}_1(0) = -0.306(14); \quad \beta = 689(133)\text{MeV}$$

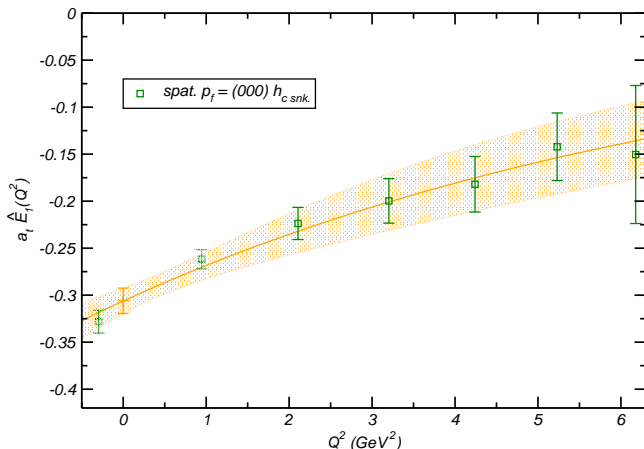


FIG. 18: $h_c \rightarrow \eta_c \gamma$ E_1 transition form-factor

The relation to the width is

$$\Gamma(h_c \rightarrow \eta_c \gamma) = \alpha \frac{|\vec{q}|}{m_{h_c}^2} \frac{16}{27} |\hat{E}_1(0)|^2,$$

so that we predict

$$\Gamma(h_c \rightarrow \eta_c \gamma) = \frac{663(132)}{601(55)} \text{keV}.$$

where the upper value uses lattice masses and the lower value physical masses.

The C_1 multipole is displayed in figure 19 with the same fit form used for the $\chi_{c0} \rightarrow J/\psi\gamma$ transition.

$$a_t \tilde{c} = -2.90(18); \quad \beta = 545(49)\text{MeV}$$

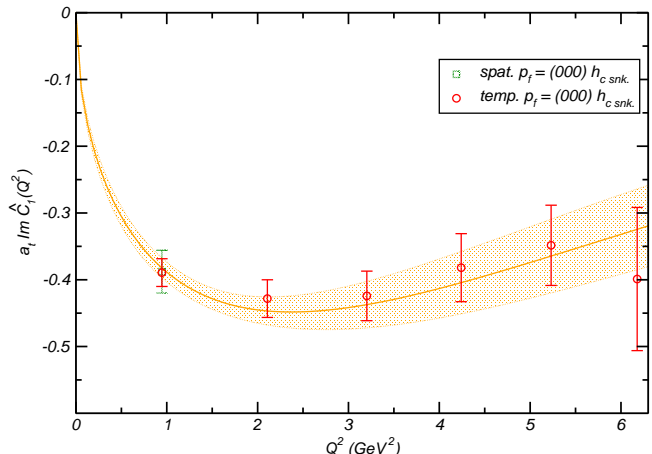


FIG. 19: $h_c \rightarrow \eta_c \gamma$ C_1 transition form-factor

VII. DISCUSSION

We extracted, for the first time, a (limited) charmonium spectrum using domain wall fermions on an anisotropic lattice. While an imperfect quark mass tuning left our spectrum systematically 5% too light, the gross features of the S & P levels were correct and notably we found a rather large hyperfine splitting in contrast to other quenched improved actions.

By attaching a vector current to only the quark line and not the antiquark, we avoided the constraint of charge conjugation invariance and sampled the vector form-factors of the lightest three charmonium states. The charge form-factors of the η_c and J/ψ were similar as expected, and, as one might anticipate on the basis of dispersion relations, did not appear to be dominated by a single VMD mechanism.

For the J/ψ the magnetic dipole form-factor was extrapolated back to $Q^2 = 0$ to yield a magnetic dipole moment that was consistent with there being zero anomalous charm quark magnetic moment in a quark model picture. Similarly the very small quadrupole moment extracted indicated minimal D -wave admixture into the J/ψ . The χ_{c0} form-factor displayed a larger charge radius than the η_c , indicating the effect of the centrifugal barrier in the P -wave state.

In Table II we summarise our results for radiative transitions, where it is clear that the β values for the $P \rightarrow S$ transitions are all compatible with having the same value, which is in line with quark model expectations that the χ_{cJ}, h_c spatial wavefunctions should differ only through small spin-orbit distortions (and perhaps differing closed-channel effects if these are allowed

for[51, 52]⁸). Within (p)NRQCD one might also have differing color octet contributions[41].

E1	$\chi_{c0} \rightarrow J/\psi\gamma$	$\chi_{c1} \rightarrow J/\psi\gamma$	$h_c \rightarrow \eta_c\gamma$
β/MeV	542(35)	555(113)	689(133)
ρ/MeV	1080(130)	1650(590)	∞
$\Gamma_{\text{phys.mass}}^{\text{lat.mass}}/\text{keV}$	288(60)	600(178)	663(132)
	232(41)	487(122)	601(55)
$\Gamma_{\text{CLEO}}^{\text{PDG}}/\text{keV}$	115(14)	303(44)	-
	204(31)	364(31)	-
M1	$J/\psi \rightarrow \eta_c\gamma$	M2	$\chi_{c1} \rightarrow J/\psi\gamma$
β/MeV	540(10)	β/MeV	617(142)
$\Gamma_{\text{phys.mass}}^{\text{lat.mass}}/\text{keV}$	1.61(7)	$\frac{M_2}{E_1}$	-0.199(121)
	2.57(11)		
$\Gamma_{\phi\phi}^{\text{PDG}}/\text{keV}$	1.14(33)	expt.	-0.002($^{+8}_{-17}$)
	2.9(1.5)		
C1	$\chi_{c0} \rightarrow J/\psi\gamma$	$\chi_{c1} \rightarrow J/\psi\gamma$	$h_c \rightarrow \eta_c\gamma$
β/MeV	501(33)	502(38)	545(49)
$ \tilde{c} /\text{GeV}$	11(1)	17.6(1.6)	17.5(1.1)

TABLE II: Radiative transitions

We can also compare the pattern of ρ values for the E_1 transitions with the expectations of a simple quark model. Performing a non-relativistic reduction of the vector current, the ρ term arises from the spin-dependent correction ($\propto \vec{\sigma} \times \vec{q}$) to the dominant convection current $\propto \vec{p}$; using effective harmonic oscillator wavefunctions one finds[53]

$$E_1^{\text{QM}}(Q^2) = a \left(1 + r \frac{|\vec{q}|^2}{4\beta_\psi^2} \right) \exp - \frac{|\vec{q}|^2}{16\beta^2}, \quad (17)$$

where r is related to spin-orbit Clebsch-Gordan coefficients,

$$r = \begin{array}{l} 2 \quad \chi_{c0} \\ 1 \quad \chi_{c1} \\ 0 \quad h_c \end{array}$$

Working in the χ_c rest frame at small Q^2 we would have $|\vec{q}|^2 \approx |\vec{q}|_0^2 + Q^2(1 + \Delta)$ where $|\vec{q}|_0 = \frac{m_\chi^2 - m_\psi^2}{2m_\chi}$ is the three-momentum transfer at $Q^2 = 0$ and $\Delta = \frac{1}{2} \left(\frac{m_\psi^2}{m_\chi^2} - 1 \right)$. Thus we can express the quark model form as

$$E_1^{\text{QM}}(Q^2) = E_1^{\text{QM}}(0) \left(1 + r \frac{Q^2}{4\beta_\psi^2} \frac{1 + \Delta}{1 + \delta} \right) \exp - \frac{Q^2(1 + \Delta)}{16\beta^2}, \quad (18)$$

with $\delta = r \frac{|\vec{q}|_0^2}{4\beta_\psi^2}$ and $E_1^{\text{QM}}(0) = a(1 + \delta) \exp - \frac{|\vec{q}|_0^2}{16\beta^2}$. Hence, to a first approximation we'd expect that $\rho \sim \frac{1}{\sqrt{\tau}}$ so that $\rho(\chi_{c1}) \approx \sqrt{2}\rho(\chi_{c0})$ and $\rho(h_c) \rightarrow \infty$. In the same approximation we have $\rho(\chi_{c0}) \approx 2\beta_\psi$. Within the large

errors on the lattice results, these relations appear to be satisfied.

Within the quark model, the M_2 transition is suppressed relative to E_1 by one power of v/c . It is also rather sensitive to any charm quark anomalous magnetic moment. Some details are worked out in [54], where they find a value (setting $\kappa_c = 0$) $M_2(0)/E_1(0) \sim -0.06$. Our data is unfortunately not sufficiently accurate to discriminate on this level - we outlined earlier in the text some possible improvements to the calculation to remedy this.

In this first attempt at charmonium radiative transitions using lattice QCD we have demonstrated that it is possible to get reasonable agreement with experiment and have gone some way to justifying certain results of the more widely applied quark model. Future lattice work in this direction will have to address the problem of reliable excited state extraction in order to consider such well-measured transitions as $\psi' \rightarrow \chi_{cJ}\gamma$.

There is, naturally, a desire to see calculations done without the quenched approximation, but, as discussed in section II, we do not expect unquenching to affect radiative transitions particularly strongly, except in the sense that it will improve the lattice state masses and help remove the phase-space ambiguity we encountered in section VI. However, an unquenched computation is warranted to test models which propose a considerable effect from coupled channels[51].

Our ultimate aim is to study photocouplings of light-quark hybrid mesons, with this in mind the next step will be to consider radiative transitions involving charmonium hybrids - the non-local interpolating fields required for this study will also allow us to access higher spin conventional charmonia such as the χ_{c2} .

Acknowledgments

We thank Eric Swanson, Olga Lakhina, Frank Close, Ted Barnes and Jim Napolitano for discussions.

This work was supported by DOE contract DE-AC05-84ER40150 under which the Southeastern Universities Research Association operates the Thomas Jefferson National Accelerator Facility. Computations were performed on clusters at Jefferson Laboratory under the SciDAC initiative.

APPENDIX A: MULTIPOLE DECOMPOSITION

It is convenient to express radiative transition amplitudes in terms of multipoles. In this appendix we derive Lorentz covariant decompositions of vector current matrix elements into multipoles. These decompositions do not appear to have been explicitly presented previously in the literature.

Our method involves writing down the most general Lorentz covariant, current conserving and parity invariant decomposition of the matrix element of the current

⁸ But note that such effects are not present within our quenched calculation

in terms of a number of arbitrary form-factors. We then compute the helicity amplitudes for the decay $i \rightarrow f\gamma$ by contracting the current matrix element with a photon polarisation vector. For convenience we work in a particular frame, but the result is covariant. The relationship between helicity amplitudes and multipoles is prescribed

in [55], whence we eliminate the arbitrary form-factors in favour of the multipole form-factors.

We will demonstrate the method with the scalar-vector transition ($0^+ \leftrightarrow 1^-$) relevant to $\chi_{c0} \rightarrow J/\psi\gamma$. The most general Lorentz covariant decomposition is:

$$\begin{aligned} \langle S(\vec{p}_S) | j^\mu(0) | V(\vec{p}_V, r) \rangle \\ = A(q^2) \epsilon^{\mu\rho\sigma\tau} \epsilon_\rho(\vec{p}_V, r) p_{V\sigma} p_{S\tau} + P(q^2) \epsilon^\mu(\vec{p}_V, r) + [\epsilon(\vec{p}_V, r) \cdot p_S] \left[B_+(q^2) (p_S + p_V)^\mu + B_-(q^2) (p_S - p_V)^\mu \right], \end{aligned} \quad (\text{A1})$$

where the polarisation vectors carry a label r which is the z -component of the spin (which is not equal to the helicity in general).

Parity invariance requires that

$$\begin{aligned} \langle S(\vec{p}_S) | j^\mu(0) | V(\vec{p}_V, r) \rangle &= \langle S(\vec{p}_S) | \mathcal{P}^{-1} \mathcal{P} j^\mu(0) \mathcal{P}^{-1} \mathcal{P} | V(\vec{p}_V, r) \rangle \\ &= -\mathbf{P}_V^\mu \langle S(-\vec{p}_S) | j^\nu(0) | V(-\vec{p}_V, r) \rangle, \end{aligned}$$

where we've used $\mathcal{P} | S(\vec{p}_S) \rangle = | S(-\vec{p}_S) \rangle$, $\mathcal{P} | V(\vec{p}_V, r) \rangle = -| V(-\vec{p}_V, r) \rangle$ and $\mathcal{P}^{-1} j^\mu \mathcal{P} = \mathbf{P}_V^\mu j^\nu$ ⁹. Hence

$$\begin{aligned} A(q^2) \epsilon^{\mu\rho\sigma\tau} \epsilon_\rho(\vec{p}_V, r) p_{V\sigma} p_{S\tau} + P(q^2) \epsilon^\mu(\vec{p}_V, r) + [\epsilon(\vec{p}_V, r) \cdot p_S] \left[B_+(q^2) (p_S + p_V)^\mu + B_-(q^2) (p_S - p_V)^\mu \right] \\ = -\mathbf{P}_V^\mu \left(A(q^2) \epsilon^{\nu\rho\sigma\tau} \epsilon_\rho(-\vec{p}_V, r) (\mathbf{P} p_V)_\sigma (\mathbf{P} p_S)_\tau + P(q^2) \epsilon^\nu(-\vec{p}_V, r) \right. \\ \left. + [\epsilon(-\vec{p}_V, r) \cdot (\mathbf{P} p_S)] \left[B_+(q^2) (\mathbf{P} p_S + \mathbf{P} p_V)^\nu + B_-(q^2) (\mathbf{P} p_S - \mathbf{P} p_V)^\nu \right] \right). \end{aligned}$$

Properties of the rotation group give that $\epsilon^\mu(-\vec{p}, r) = -\mathbf{P}_V^\mu \epsilon^\nu(\vec{p}, r)$ using which one verifies the parity invariance of this decomposition provided $A(q^2) = 0$.

The conservation of the vector current is an additional constraint,

$$\begin{aligned} 0 &= \partial_\mu \langle S(\vec{p}_S) | j^\mu(x) | V(\vec{p}_V, r) \rangle \\ &= \partial_\mu \langle S(\vec{p}_S) | e^{i\vec{p} \cdot x} j^\mu(0) e^{-i\vec{p} \cdot x} | V(\vec{p}_V, r) \rangle \\ &= \partial_\mu e^{i(p_S - p_V) \cdot x} \langle S(\vec{p}_S) | j^\mu(0) | V(\vec{p}_V, r) \rangle \\ \implies 0 &= q_\mu \langle S(\vec{p}_S) | j^\mu(0) | V(\vec{p}_V, r) \rangle, \end{aligned}$$

whence we eliminate one of the three form-factors,

$$P(q^2) = (m_V^2 - m_S^2) B_+(q^2) - q^2 B_-(q^2).$$

Multipole amplitudes are most easily defined in terms of helicity amplitudes which can be obtained from the decompositions of the previous section in a straightforward way. First we will find the defining relation for multipole amplitudes in terms of helicity amplitudes. This is done in analogy with Durand [55], but rather than working in the Breit frame we choose to work in the rest frame of the decaying particle. The results are Lorentz covariant so this choice of frame is irrelevant.

We can define a vertex function in the rest frame of a

particle of spin- J

$$\begin{aligned} \Gamma^\nu(J'\lambda'; J\lambda) &\equiv \langle p'\hat{z}; J'\lambda' | j^\nu | J\lambda \rangle \\ &= \langle J'\lambda' | e^{i\xi_{p'} K_3} j^\nu | J\lambda \rangle, \end{aligned} \quad (\text{A2})$$

where $|p'\hat{z}; J'\lambda'\rangle$ is a final state of spin- J' , *helicity*- λ' in motion along the positive z -axis with momentum p' , $|J\lambda\rangle$ is a similar (initial) state at rest and $e^{i\xi_{p'} K_3}$ is the unitary operator effecting the boost from rest to momentum $p'\hat{z}$. The matrix element (A1) discussed in the previous section is a generalisation of this vertex functions to an arbitrary Lorentz frame, i.e. $\Gamma^\mu(0, 0; 1, \lambda) = \langle S(p'\hat{z}) | j^\mu(0) | V(\vec{0}, r = \lambda) \rangle$. Note that now we are opting to use helicity and not the z -component of angular momentum. However since we have chosen the end-state particle to move along the positive z -direction, we have $\lambda = r, \lambda' = r'$.

In this frame the amplitude for the decay $(J\lambda) \rightarrow (J'\lambda') + (\gamma\lambda_\gamma)$ is

$$\mathcal{M} = \epsilon_\nu^*(-p'\hat{z}, \lambda_\gamma) \Gamma^\nu(J'\lambda'; J\lambda),$$

where the polarisation vectors for a photon moving along the ($-z$)-direction are

$$\begin{aligned} \epsilon^\mu(-p'\hat{z}, \lambda_\gamma = \pm) &= \pm \frac{1}{\sqrt{2}} (0, 1, \mp i, 0) \\ \epsilon^\mu(-p'\hat{z}, \lambda_\gamma = 0) &= \frac{1}{\sqrt{q^2}} (p', 0, 0, -\sqrt{p'^2 + q^2}). \end{aligned}$$

We find that

$$\mathcal{M}(\lambda_\gamma) = \delta_{\lambda, \lambda' - \lambda_\gamma} c_{\lambda_\gamma} \Gamma^{\lambda_\gamma}(J' \lambda'; J \lambda),$$

where $c_\pm = 1$, $c_0 = -\frac{\sqrt{q^2}}{p'}$ and $\Gamma^\pm \equiv \mp \frac{1}{\sqrt{2}}(\Gamma^1 \pm i\Gamma^2)$.

Returning to the definition of the vertex function (A2), we assert that $e^{i\xi_{p'} K_3} j^\nu$ can be expressed as a sum of operators which transform as tensors under the rotation group - this is the essence of a multipole expansion: $e^{i\xi_{p'} K_3} j^\nu = \sum_k T_{(\nu)}^k$. The vertex operator is then a sum of matrix elements of these tensors, each of which satisfies the Wigner-Eckart theorem, so that, for all spins integral, we can write

$$\Gamma^\nu(J' \lambda'; J \lambda) = \sum_k (-1)^{J' + \lambda'} \begin{pmatrix} J' & k & J \\ -\lambda' & \nu & \lambda \end{pmatrix} \langle J' || T_{(\nu)}^k || J \rangle,$$

where $\nu = \pm, 0$. j^0 and j^\pm are in different representations of the rotation group, so we'll allow different reduced matrix elements for each. A purely conventional redefinition of the reduced matrix element is $\langle J' || T_{(\pm)}^k || J \rangle = (-1)^k \sqrt{2k+1} [E_k \frac{1}{2}(1 + (-1)^k \delta P) \mp M_k \frac{1}{2}(1 - (-1)^k \delta P)]$ for the transverse case and $\langle J' || T_{(0)}^k || J \rangle = \frac{p'}{\sqrt{q^2}} (-1)^{k+1} \sqrt{(2k+1)} C_k \frac{1}{2} (1 + (-1)^k \delta P)$ for the longitudinal case¹⁰. δP is the product of initial and final meson parities and $E(M)$ indicates an electric(magnetic) multipole. After some manipulation we obtain the multipole decomposition of the helicity amplitudes,

$$\begin{aligned} \mathcal{M}(\lambda_\gamma = \pm) &= \sum_k \sqrt{\frac{2k+1}{2J+1}} [E_k \frac{1}{2}(1 + (-1)^k \delta P) \mp M_k \frac{1}{2}(1 - (-1)^k \delta P)] \langle k \mp; J' \lambda \pm 1 | J \lambda \rangle \\ \mathcal{M}(\lambda_\gamma = 0) &= \sum_k \sqrt{\frac{2k+1}{2J+1}} C_k \frac{1}{2} (1 + (-1)^k \delta P) \langle k 0; J' \lambda | J \lambda \rangle. \end{aligned}$$

For the particular case under study, $J = 0, J' = 1$; this transition has one transverse multipole - E_1 and one longitudinal multipole - C_1 .

$$\begin{aligned} \mathcal{M}(\lambda_\gamma = \pm) &= E_1(q^2) \\ \mathcal{M}(\lambda_\gamma = 0) &= -C_1(q^2) \end{aligned} \quad (\text{A3})$$

Contracting the complex conjugate of (A1) with a photon polarisation vector yields,

$$\begin{aligned} \mathcal{M}(\lambda_\gamma = \pm) &= (m_V^2 - m_S^2) B_+(q^2) - q^2 B_-(q^2) \\ \mathcal{M}(\lambda_\gamma = 0) &= -\frac{\sqrt{q^2}}{2m_V} [(m_V^2 - m_S^2 + q^2) B_-(q^2) - (3m_V^2 + m_S^2 - q^2) B_+(q^2)] \end{aligned} \quad (\text{A4})$$

Solving (A3), (A4) for $B_\pm(q^2)$ allows us to write the current matrix element as a multipole expansion.

$$\begin{aligned} \langle S(\vec{p}_S) | j^\mu(0) | V(\vec{p}_V, r) \rangle &= \Omega^{-1}(q^2) \left(E_1(q^2) \left[\Omega(q^2) \epsilon^\mu(\vec{p}_V, r) - \epsilon(\vec{p}_V, r) \cdot p_S (p_V^\mu p_V \cdot p_S - m_V^2 p_S^\mu) \right] \right. \\ &\quad \left. + \frac{C_1(q^2)}{\sqrt{q^2}} m_V \epsilon(\vec{p}_V, r) \cdot p_S [p_V \cdot p_S (p_V + p_S)^\mu - m_S^2 p_V^\mu - m_V^2 p_S^\mu] \right) \end{aligned} \quad (\text{A5})$$

Note that this is expressed entirely in terms of invariants and covariant quantities and hence can be used in any frame. One can check that the tensor coefficients of the form-factors are orthogonal, indicating the independence of E_1, C_1 . The invariant quantity $\Omega(q^2) \equiv (p_V \cdot p_S)^2 - m_V^2 m_S^2 = \frac{1}{4} [(m_V - m_S)^2 - q^2] [(m_V + m_S)^2 - q^2]$, and takes the simple value $m_S^2 |\vec{q}|^2$ in the rest frame of the decaying scalar.

The decomposition is further constrained by

Minkowski time-reversal invariance of the matrix element; this is a symmetry of the system if the meson states are stable. Time-reversal is implemented as an anti-unitary operation (\mathcal{T}). As such the statement of invariance for the matrix element of a hermitian operator is $\langle \beta | A | \alpha \rangle = \langle \tilde{\alpha} | \mathcal{T} A \mathcal{T}^{-1} | \tilde{\beta} \rangle = (\langle \tilde{\beta} | \mathcal{T} A \mathcal{T}^{-1} | \tilde{\alpha} \rangle)^*$ where $|\tilde{\alpha}\rangle = \mathcal{T} |\alpha\rangle$. States of definite momentum, spin and z -component of spin transform as $\mathcal{T} |\vec{p}, J, r\rangle = \zeta (-1)^{J-r} |-\vec{p}, J, -r\rangle$, where ζ is an

arbitrary unphysical phase that we can choose independently for each particle type[56]. For the scalar and vector we choose $\zeta = +1$ - with this the vector has a real decay constant, f_V defined in the standard way: $\langle 0|\bar{\psi}(0)\gamma^\mu\psi(0)|V(\vec{q}, r)\rangle = m_V f_V \epsilon^\mu(\vec{q}, r)$. Note that to get a real pseudoscalar decay constant one needs to choose $\zeta_P = -1$ (see the next appendix).

The vector current transforms as $\mathcal{T}j^\mu\mathcal{T}^{-1} = \mathbf{P}_\nu^\mu j^\nu$. Using the relation $\epsilon^{\mu*}(\vec{p}, r) = (-1)^{r+1}\mathbf{P}_\nu^\mu \epsilon^\nu(-\vec{p}, -r)$ one can show that $E_1(q^2)$ and $\frac{C_1(q^2)}{\sqrt{q^2}}$ are real.

An equivalent procedure for the axial-vector transition ($1^+ \leftrightarrow 1^-$) yields the decomposition

$$\begin{aligned} \langle A(\vec{p}_A, r_A)|j^\mu(0)|V(\vec{p}_V, r_V)\rangle &= \frac{i}{4\sqrt{2}\Omega(q^2)}\epsilon^{\mu\nu\rho\sigma}(p_A - p_V)_\sigma \times \\ &\times \left[E_1(q^2)(p_A + p_V)_\rho \left(2m_A[\epsilon^*(\vec{p}_A, r_A)\cdot p_V]\epsilon_\nu(\vec{p}_V, r_V) + 2m_V[\epsilon(\vec{p}_V, r_V)\cdot p_A]\epsilon_\nu^*(\vec{p}_A, r_A) \right) \right. \\ &+ M_2(q^2)(p_A + p_V)_\rho \left(2m_A[\epsilon^*(\vec{p}_A, r_A)\cdot p_V]\epsilon_\nu(\vec{p}_V, r_V) - 2m_V[\epsilon(\vec{p}_V, r_V)\cdot p_A]\epsilon_\nu^*(\vec{p}_A, r_A) \right) \\ &+ \frac{C_1(q^2)}{\sqrt{q^2}} \left(-4\Omega(q^2)\epsilon_\nu^*(\vec{p}_A, r_A)\epsilon_\rho(\vec{p}_V, r_V) \right. \\ &\left. \left. + (p_A + p_V)_\rho \left[(m_A^2 - m_V^2 + q^2)[\epsilon^*(\vec{p}_A, r_A)\cdot p_V]\epsilon_\nu(\vec{p}_V, r_V) + (m_A^2 - m_V^2 - q^2)[\epsilon(\vec{p}_V, r_V)\cdot p_A]\epsilon_\nu^*(\vec{p}_A, r_A) \right] \right) \right] \end{aligned} \quad (\text{A6})$$

APPENDIX B: MINKOWSKI AND EUCLIDEAN N-POINT FUNCTIONS

We obtained all our Lorentz decompositions in Minkowski space, but perform lattice computation in Euclidean; in this appendix we outline a simple way to effect the mapping between the two and describe some discrete symmetry constraints.

1. Two-point functions

In Minkowski space the following fermion bilinears are hermitian:

$$\begin{aligned} S(x) &= \bar{\psi}(x)\psi(x) \\ P(x) &= \bar{\psi}(x)i\gamma^5\psi(x) \\ V^\mu(x) &= \bar{\psi}(x)\gamma^\mu\psi(x) \\ A^\mu(x) &= \bar{\psi}(x)\gamma^\mu\gamma^5\psi(x) \\ T^{\mu\nu}(x) &= \bar{\psi}(x)\sigma^{\mu\nu}\psi(x). \end{aligned} \quad (\text{B1})$$

The transformation of spin-0 and spin-1 fields under time-reversal can be written

$$\begin{aligned} \mathcal{T}\varphi(x)\mathcal{T}^{-1} &= \zeta_\varphi^*\varphi(-Px); \\ \mathcal{T}v^\mu(x)\mathcal{T}^{-1} &= \zeta_v^*\mathbf{P}_\nu^\mu v^\nu(-Px), \end{aligned}$$

with arbitrary phases ζ . The choices in (B1) correspond to

$$\zeta_S = +1; \quad \zeta_P = -1; \quad \zeta_V = +1; \quad \zeta_A = +1,$$

so that the decay constants defined in (5) are real:

$$\begin{aligned} iq^\mu f_P &= (\mathbf{P}_\nu^\mu \zeta_P \langle 0|\bar{\psi}(0)\gamma^\nu\gamma^5\psi(0)|P(-\vec{q})\rangle)^* \\ &= -i\mathbf{P}_\nu^\mu \mathbf{P}_\rho^\nu q^\rho f_P^* \zeta_P \\ \implies f_P &= f_P^*, \\ m_V f_V \epsilon^\mu(\vec{q}, r) &= (\mathbf{P}_\nu^\mu \zeta_V (-1)^{1-r} \langle 0|\bar{\psi}(0)\gamma^\nu\psi(0)|V(-\vec{q}, -r)\rangle)^* \\ &= \zeta_V (-1)^{1-r} m_V f_V^* \mathbf{P}_\nu^\mu \epsilon^{\nu*}(-\vec{q}, -r) \\ \implies f_V &= f_V^*. \end{aligned}$$

In addition, the overlap factors Z must be real:

$$\begin{aligned} Z_P(\vec{p}) &\equiv \langle 0|\bar{u}i\gamma^5 d(\vec{0}, 0)|P(\vec{p})\rangle \\ &= (\langle 0|\mathcal{T}^{-1}\mathcal{T}\bar{u}i\gamma^5 d(\vec{0}, 0)\mathcal{T}^{-1}\mathcal{T}|P(\vec{p})\rangle)^* \\ &= (\langle 0|(-1)\bar{u}i\gamma^5 d(\vec{0}, 0)\zeta_P|P(-\vec{p})\rangle)^* = Z_P^*(-\vec{p}), \end{aligned}$$

since for the truly local operator, Z is not actually a function of \vec{p} and where for a rotationally-invariant smeared operator $Z = Z(|\vec{p}|)$.

The mapping between Minkowski and Euclidean spacetimes is effected by the transformations,

$$\begin{aligned} t &\rightarrow -i\tilde{t} \\ \gamma^0 &\rightarrow \tilde{\gamma}_4 \\ \gamma^k &\rightarrow i\tilde{\gamma}_k \\ \gamma^5 &\rightarrow -\tilde{\gamma}_5, \end{aligned} \quad (\text{B2})$$

where the tilded quantities are Euclidean (e.g. the gamma matrices satisfy $\{\tilde{\gamma}_\mu, \tilde{\gamma}_\nu\} = 2\delta_{\mu\nu}$).

Consider as an example the vector two-point function in Minkowski space,

$$\begin{aligned}\Gamma^{(2)ij}(\vec{p}, t) &= \sum_{\vec{x}} e^{i\vec{p}\cdot\vec{x}} \langle \bar{\psi} \gamma^i \psi(\vec{x}, t) [\bar{\psi} \gamma^j \psi(\vec{0}, 0)]^\dagger \rangle \\ &= \sum_N \frac{(Z_\psi^{(N)})^2}{2E_\psi^{(N)}} e^{-iE_\psi^{(N)}t} \sum_r \epsilon^i(\vec{p}, r) \epsilon^{*j}(\vec{p}, r) \\ &= \sum_N \frac{(Z_\psi^{(N)})^2}{2E_\psi^{(N)}} e^{-iE_\psi^{(N)}t} \left(\delta_{ij} + \frac{p^i p^j}{(m_\psi^{(N)})^2} \right),\end{aligned}$$

where we inserted a complete set of states and used the Minkowski space completeness expression for polarisation vectors $\sum_r \epsilon^\mu(\vec{p}, r) \epsilon^{*\nu}(\vec{p}, r) = \left(-g^{\mu\nu} + \frac{p^\mu p^\nu}{p^2} \right)$. In the lattice calculation we actually compute a Euclidean quantity:

$$\begin{aligned}\tilde{\Gamma}_{ij}^{(2)}(\vec{p}, \tilde{t}) &= - \left\langle \sum_{\vec{x}} e^{i\vec{p}\cdot\vec{x}} \text{tr} \left\{ (\tilde{\gamma}_5 G(x, 0) \tilde{\gamma}_5)^\dagger \tilde{\gamma}_j G(x, 0) \tilde{\gamma}_i \right\} \right\rangle \\ &= \sum_{\vec{x}} e^{i\vec{p}\cdot\vec{x}} \langle \bar{\psi} \tilde{\gamma}_i \psi(\vec{x}, t) \bar{\psi} \tilde{\gamma}_j \psi(\vec{0}, 0) \rangle \\ &= (-i)^2 \Gamma^{(2)ij}(\vec{p}, -i\tilde{t}) \\ &= - \sum_N \frac{(Z_\psi^{(N)})^2}{2E_\psi^{(N)}} e^{-E_\psi^{(N)}\tilde{t}} \left(\delta_{ij} + \frac{p^i p^j}{(m_\psi^{(N)})^2} \right),\end{aligned}$$

where with this derivation it is clear that all energies and momentum should be interpreted as the usual real Minkowski variants. All that we had to do was apply the mapping (B2). Note that we only ever consider polarisation vectors in Minkowski space, where they are easily defined.

2. Three-point functions

In Minkowski space, inserting two complete sets of states gives

$$\begin{aligned}\Gamma^{(3)f\Gamma i}(\vec{p}_f, \vec{q}; t_f, t) &= \sum_{f,i} \frac{e^{-iE_f t_f} e^{-i(E_i - E_f)t}}{2E_f(\vec{p}_f) 2E_i(\vec{p}_i)} \\ &\quad \langle 0 | \bar{\psi} \Gamma_f \psi(\vec{0}, 0) | f(\vec{p}_f, r_f) \rangle \langle f(\vec{p}_f, r_f) | \bar{\psi} \Gamma \psi(\vec{0}, 0) | i(\vec{p}_i, r_i) \rangle \left(\langle 0 | \bar{\psi} \Gamma_i \psi(\vec{0}, 0) | i(\vec{p}_i, r_i) \rangle \right)^*.\end{aligned}$$

The Minkowski space-time Lorentz decomposition of the matrix element was discussed in the previous appendix. We actually compute the Euclidean variant,

$$\tilde{\Gamma}_{f\Gamma i}^{(3)}(\vec{p}_f, \vec{q}; \tilde{t}_f, \tilde{t}) = c_f c_{\Gamma i} \Gamma^{(3)f\Gamma i}(\vec{p}_f, \vec{q}; -i\tilde{t}_f, -i\tilde{t})$$

where e.g. $\tilde{\Gamma}_i = c_i \Gamma^i$. As an explicit example consider the η_c form-factor where $\Gamma_f = \Gamma_i = i\gamma^5$ and $\Gamma = \gamma^\mu$. Then using (B2) we have

$$\begin{aligned}\Gamma^{(3)P\gamma^k P}(\vec{p}_f, \vec{q}; -i\tilde{t}_f, -i\tilde{t}) &= \text{Im} \tilde{\Gamma}_{P\gamma^k P}^{(3)}(\vec{p}_f, \vec{q}; \tilde{t}_f, \tilde{t}) \\ \Gamma^{(3)P\gamma^0 P}(\vec{p}_f, \vec{q}; -i\tilde{t}_f, -i\tilde{t}) &= -\text{Re} \tilde{\Gamma}_{P\gamma^0 P}^{(3)}(\vec{p}_f, \vec{q}; \tilde{t}_f, \tilde{t}).\end{aligned}$$

One should perform the mapping on each transition computed to ensure that one extracts the correct complex component with the right sign.

APPENDIX C: SCALE SETTING ON ANISOTROPIC LATTICES

We outline how to set the scale of dimensionful quantities when one has differing spatial and temporal lattice spacings. The lattice action, written in terms of dimensionful quantities is $S = \sum_{x^\mu} a_s^3 a_t \bar{\psi} Q \psi$. If we scale the fermion fields by $\check{\psi} = a_s^{3/2} \psi$ then we get a lattice spacing independent action, $\sum_{x^\mu} \check{\psi} \check{Q} \check{\psi}$, if $\check{Q} = a_t Q$ where the anisotropy will appear in the spatial derivative operator.

On the anisotropic lattice a bosonic field would have a mass term in the action proportional to $\sum_{x^\mu} a_s^3 a_t m^2 \phi^2$, so that if we scale the mass as $\check{m} = a_t m$ (as we must since it appears in Euclidean correlators like e^{-mt}), then we have to scale the boson field as $\check{\phi} = \sqrt{\frac{a_s^3}{a_t}} \phi$.

If we define the creation/annihilation operators by the

continuum decomposition¹¹

$$\phi(x) = \int \frac{d^3\vec{p}}{(2\pi)^3} \frac{1}{2E_{\vec{p}}} (\alpha^\dagger(\vec{p})e^{ip \cdot x} + \alpha(\vec{p})e^{-ip \cdot x}),$$

and use $p_i = \frac{2\pi}{L_i a_s} n_i$ (3-momenta must scale with a_s as they appear in the dimensionless combination $\vec{p} \cdot \vec{x}$) we have

$$\phi(x) = \sqrt{\frac{a_t}{a_s^3}} \check{\phi} = \sum_{\vec{n}_p} \frac{1}{L^3 a_s^3} \frac{a_t}{2\check{E}_{\vec{p}}} (\alpha^\dagger(\vec{p})e^{ip \cdot x} + \alpha(\vec{p})e^{-ip \cdot x}),$$

so that the dimensionless creation/annihilation operator is $\check{\alpha} = \sqrt{\frac{a_t}{a_s^3}} \alpha$. Then since a single particle state is defined by $|N(\vec{p})\rangle = \alpha^\dagger|0\rangle$, we define a dimensionless single particle state by $|\check{N}(\vec{p})\rangle = \check{\alpha}^\dagger|0\rangle = \sqrt{\frac{a_t}{a_s^3}}|N(\vec{p})\rangle$. It is easy to check that the resolution of the identity takes the following form

$$\begin{aligned} 1 &= \sum_N \int \frac{d^3\vec{p}}{(2\pi)^3} \frac{1}{2E_{\vec{p}}} |N(\vec{p})\rangle \langle N(\vec{p})| \\ &\rightarrow L^{-3} \sum_N \sum_{\vec{n}_p} \frac{1}{2\check{E}_{\vec{p}}} |\check{N}(\vec{p})\rangle \langle \check{N}(\vec{p})|, \end{aligned}$$

which has no dependence on either lattice spacing. One can then show by insertion of the complete set of states that the two-point function calculated in a lattice simulation is, as expected,

$$\check{\Gamma}^{(2)} = \frac{\check{Z}^2}{2\check{E}} e^{-\check{t}\check{E}}$$

The scaling of Z is easily found

$$Z e^{-i\vec{p} \cdot \vec{x}} \equiv \langle 0 | \bar{\psi} \Gamma \psi(x) | N(\vec{p}) \rangle \rightarrow \frac{1}{\sqrt{a_s^3 a_t}} \langle 0 | \check{\bar{\psi}} \Gamma \check{\psi}(x) | \check{N}(\vec{p}) \rangle,$$

so that the dimensionless \check{Z} that appears in the lattice simulation is $\check{Z} = \sqrt{a_s^3 a_t} Z$.

The pseudoscalar decay constant, f_P , has mass dimension 1 and is defined by

$$\langle 0 | \bar{\psi}(0) \gamma^\mu \gamma^5 \psi(0) | P(\vec{q}) \rangle = i f_P q^\mu.$$

Taking the temporal component and scaling to dimensionless quantities we have

$$\frac{1}{\sqrt{a_s^3 a_t}} \langle 0 | \check{\bar{\psi}}(0) \gamma^0 \gamma^5 \check{\psi}(0) | \check{P}(\vec{q}) \rangle = i f \check{E}_{\vec{q}} a_t^{-1},$$

so that $\check{f}_P = \sqrt{\frac{a_s^3}{a_t}} f_P$. Thus to obtain the physical decay constant from the lattice value we calculate

$$f = \xi^{-3/2} a_t^{-1} \check{f}.$$

The same formula applies to the vector decay constant.

As an example of setting the scale of a dimensionful transition form-factor factor, consider the scalar to vector transition:

$$\langle S(\vec{p}_S) | \bar{\psi} \gamma^\mu \psi | V(\vec{p}_V, r) \rangle = E_1(Q^2) \epsilon^\mu(\vec{p}_V, r) + \dots$$

The LHS scales to the dimensionless version leaving only one factor of a_t in the denominator and hence $\check{E}_1 = a_t E_1$.

-
- [1] N. Brambilla et al. (2004), hep-ph/0412158.
[2] E. S. Swanson (2006), hep-ph/0601110.
[3] S. Eidelman et al. (Particle Data Group), Phys. Lett. **B592**, 1 (2004).
[4] N. E. Adam et al. (CLEO), Phys. Rev. Lett. **94**, 232002 (2005), hep-ex/0503028.
[5] V. A. Beilin and A. V. Radyushkin, Nucl. Phys. **B260**, 61 (1985).
[6] A. R. Dzierba, eConf **C010430**, T04 (2001), hep-ex/0106010.
[7] F. E. Close and J. J. Dudek, Phys. Rev. **D69**, 034010 (2004), hep-ph/0308098.
[8] F. E. Close and J. J. Dudek, Phys. Rev. Lett. **91**, 142001 (2003), hep-ph/0304243.
[9] R. G. Edwards and B. Joo (SciDAC), Nucl. Phys. Proc. Suppl. **140**, 832 (2005), hep-lat/0409003.
[10] T. R. Klassen, Nucl. Phys. **B533**, 557 (1998), hep-lat/9803010.
[11] S. Choe et al. (QCD-TARO), JHEP **08**, 022 (2003), hep-lat/0307004.
[12] I. T. Drummond, N. A. Goodman, R. R. Horgan, H. P. Shanahan, and L. C. Stoni, Phys. Lett. **B478**, 151 (2000), hep-lat/9912041.
[13] Y. Shamir, Nucl. Phys. **B406**, 90 (1993), hep-lat/9303005.
[14] R. G. Edwards and U. M. Heller, Phys. Rev. **D63**, 094505 (2001), hep-lat/0005002.
[15] T. R. Klassen, Nucl. Phys. Proc. Suppl. **73**, 918 (1999), hep-lat/9809174.
[16] P. Chen, Phys. Rev. **D64**, 034509 (2001), hep-lat/0006019.
[17] S. Gottlieb et al., PoS **LAT2005**, 203 (2005), hep-lat/0510072.
[18] C. T. H. Davies et al. (HPQCD), Phys. Rev. Lett. **92**, 022001 (2004), hep-lat/0304004.
[19] M. Albanese et al. (APE), Phys. Lett. **B192**, 163 (1987).
[20] S. Tamhankar et al. (2005), hep-lat/0507027.
[21] M. di Pierro et al., Nucl. Phys. Proc. Suppl. **129**, 340 (2004), hep-lat/0310042.
[22] C. McNeile and C. Michael (UKQCD), Phys. Rev. **D70**, 034506 (2004), hep-lat/0402012.
[23] P. de Forcrand et al. (QCD-TARO), JHEP **08**, 004 (2004), hep-lat/0404016.
[24] M. Okamoto et al. (CP-PACS), Phys. Rev. **D65**, 094508 (2002), hep-lat/0112020.
[25] X. Liao and T. Manke (2002), hep-lat/0210030.

- [26] D. Ebert, R. N. Faustov, and V. O. Galkin, *Mod. Phys. Lett.* **A18**, 1597 (2003), hep-ph/0304227.
- [27] K. W. Edwards et al. (CLEO), *Phys. Rev. Lett.* **86**, 30 (2001), hep-ex/0007012.
- [28] T. Draper, R. M. Woloshyn, W. Wilcox, and K.-F. Liu, *Nucl. Phys.* **B318**, 319 (1989).
- [29] F. D. R. Bonnet, R. G. Edwards, G. T. Fleming, R. Lewis, and D. G. Richards (Lattice Hadron Physics), *Phys. Rev.* **D72**, 054506 (2005), hep-lat/0411028.
- [30] A. Holl, A. Krassnigg, C. D. Roberts, and S. V. Wright, *Int. J. Mod. Phys.* **A20**, 1778 (2005), nucl-th/0411065.
- [31] K. Barad, M. Ogilvie, and C. Rebbi, *Phys. Lett.* **B143**, 222 (1984).
- [32] T. Blum et al., *Phys. Rev.* **D69**, 074502 (2004), hep-lat/0007038.
- [33] J. J. Kelly, *Phys. Rev.* **C66**, 065203 (2002), hep-ph/0204239.
- [34] J. Carbonell, B. Desplanques, V. A. Karmanov, and J. F. Mathiot, *Phys. Rept.* **300**, 215 (1998), nucl-th/9804029.
- [35] N. Isgur, D. Scora, B. Grinstein, and M. B. Wise, *Phys. Rev.* **D39**, 799 (1989).
- [36] E. Swanson, private Communication.
- [37] J. Dudek, Ph.D. thesis, University of Oxford (2004).
- [38] N. Isgur, *Phys. Rev.* **D60**, 114016 (1999), hep-ph/9904494.
- [39] F. E. Close and E. S. Swanson, *Phys. Rev.* **D72**, 094004 (2005), hep-ph/0505206.
- [40] L. D. Landau and E. M. Lifshitz, *Quantum Mechanics, Non-Relativistic Theory* (Pergamon Press, Oxford, UK, 1958).
- [41] N. Brambilla, Y. Jia, and A. Vairo (2005), hep-ph/0512369.
- [42] J. Gaiser et al., *Phys. Rev.* **D34**, 711 (1986).
- [43] H. C. Huang et al. (Belle), *Phys. Rev. Lett.* **91**, 241802 (2003).
- [44] E. J. Eichten, K. Lane, and C. Quigg, *Phys. Rev. Lett.* **89**, 162002 (2002), hep-ph/0206018.
- [45] T. Barnes, S. Godfrey, and E. S. Swanson, *Phys. Rev.* **D72**, 054026 (2005), hep-ph/0505002.
- [46] S. Godfrey and N. Isgur, *Phys. Rev.* **D32**, 189 (1985).
- [47] M. Ambrogiani et al. (E835), *Phys. Rev.* **D65**, 052002 (2002).
- [48] M. Oreglia et al., *Phys. Rev.* **D25**, 2259 (1982).
- [49] P. Rubin et al. (CLEO), *Phys. Rev.* **D72**, 092004 (2005), hep-ex/0508037.
- [50] J. L. Rosner et al. (CLEO), *Phys. Rev. Lett.* **95**, 102003 (2005), hep-ex/0505073.
- [51] E. Eichten, K. Gottfried, T. Kinoshita, K. D. Lane, and T.-M. Yan, *Phys. Rev.* **D17**, 3090 (1978).
- [52] E. Eichten, K. Gottfried, T. Kinoshita, K. D. Lane, and T.-M. Yan, *Phys. Rev.* **D21**, 203 (1980).
- [53] F. E. Close, A. Donnachie, and Y. S. Kalashnikova, *Phys. Rev.* **D67**, 074031 (2003), hep-ph/0210293.
- [54] K. J. Sebastian, H. Grotch, and F. L. Ridener, *Phys. Rev.* **D45**, 3163 (1992).
- [55] L. Durand, P. C. DeCelles, and R. B. Marr, *Phys. Rev.* **126**, 1882 (1962).
- [56] S. Weinberg, *The Quantum theory of fields. Vol. 1: Foundations* (Cambridge University Press, Cambridge, UK, 1995).